

NASA Contractor Report 198359

1N-71
p-37

Computation of Noise Radiation From Turbofans: A Parametric Study

ORIGINAL
COLOR ILLUSTRATIONS

7

M. Nallasamy
NYMA, Inc.
Brook Park, Ohio

N95-32836

Unclass

G3/71 0062496

July 1995

Prepared for
Lewis Research Center
Under Contract NAS3-27186



National Aeronautics and
Space Administration

(NASA-CR-198359) COMPUTATION OF
NOISE RADIATION FROM TURBOFANS: A
PARAMETRIC STUDY Final Contractor
Report (NYMA) 37 p

COMPUTATION OF NOISE RADIATION FROM TURBOFANS: A PARAMETRIC STUDY

M. Nallasamy
NYMA, Inc.
Brook Park, Ohio 44142

SUMMARY

This report presents the results of a parametric study of the turbofan far-field noise radiation using a finite element technique. Several turbofan noise radiation characteristics of both the inlet and the aft ducts have been examined through the finite element solutions. The predicted far-field principal lobe angle variations with duct Mach number and cut-off ratio compare very well with the available analytical results. The solutions also show that the far-field lobe angle is only a function of cut-off ratio, and nearly independent of the mode number. These results indicate that the finite element codes are well suited for the prediction of noise radiation characteristics of a turbofan. The effects of variations in the aft duct geometry are examined. The ability of the codes to handle ducts with acoustic treatments is also demonstrated.

NOMENCLATURE

B	number of rotor blades
c	speed of sound
c_{mn}	modal amplitude
J_m	Bessel function of first kind and order m
k_{mn}	eigen value of mode (m,n)
M_d	duct Mach number
m	circumferential mode order
n	radial mode order
p	acoustic pressure
Q_{mn}	coefficient of Y_m
R	normalized resistance
r	radial coordinate
r_0	duct radius
s	harmonic number
V	number of stator vanes
v	normal component of velocity
X	normalized reactance
z	normalized impedance

ξ	cut-off ratio
ψ_p	far-field principal lobe angle
ω	frequency

INTRODUCTION

One of the major sources of noise in aircraft turbofan engines is the fan noise. The noise radiated from the fan inlet and aft ducts is of great concern during takeoff and landing. It is recognized that the fan noise is a critical component controlling the total noise at takeoff and approach conditions (ref. 1). Stringent limits on airport noise levels and curfews necessitate a better understanding of the noise generation mechanisms and the noise suppression techniques to alleviate community noise problems.

A typical fan noise spectrum consists of tone noise (blade passing frequency and its harmonics) superimposed over broadband noise. The tone noise is the result of the interaction of the periodic disturbances of the rotor blade mean (viscous) wake with stator vanes. This is usually referred to as rotor-stator interaction noise and is the component considered here. The acoustic pressure distribution in the duct can be expressed in terms of normal modes once the pressure dipole distribution on the blades is known. The blade pressure distribution is usually computed using quasi-three-dimensional techniques or strip theory which employs local two-dimensional approximations.

The generated noise may consist of propagating and nonpropagating or decaying modes. The propagating modes can travel upstream or downstream of the source plane. The sound transmission through the blade row has been studied extensively. Modal transmission and reflection have been known to be as important as the source of mode generation. The direction of rotation of the mode with respect to the direction of rotation of the rotor greatly influences its transmission/reflection properties.

The noise radiation to the far-field may be computed using analytical methods or finite volume/finite element numerical techniques. The finite volume/finite element techniques have the advantage of modeling the geometry accurately. The finite element technique is used in the present study.

An understanding of turbofan tone noise relevant to community noise thus requires consideration of rotor-stator interaction noise, propagation through the duct, transmission through the rotor and radiation to the far-field. However, in this report attention is focussed on the radiation of noise to the far-field from the inlet and aft ducts of the fan. The results of a parametric study of the inlet/aft radiation are reported. Several characteristics of the fan noise radiation pattern are examined through finite element solutions. The capability of the solution technique to handle ducts lined with sound absorbing materials is also demonstrated. The finite element technique and computer codes developed by Eversman and Roy (refs. 2 and 3) and applied to modern turbofans by Topol et al. (refs. 4 and 5) have been used in the present study.

DUCT ACOUSTICS

The idea of analyzing the fan noise in terms of the spinning pressure patterns in the fan duct first introduced by Tyler and Sofrin [6] has since influenced the fan noise research and fan acoustic design. They resolved the sound field into annular duct modes, m (number of wavelengths in the circumferential direction) and the radial order, n (number of nodes or zero crossings of pressure in the radial direction). The radial distribution of pressure in a duct is expressed in the form

$$p(r) = c_{mn} [J_m(k_{mn}r) + Q_{mn} Y_m(k_{mn}r)] \quad (1)$$

J_m and Y_m are the Bessel functions of the first and second kind respectively. k_{mn} is the eigen value of the radial wave number for (m,n) mode. k_{mn} and Q_{mn} are functions of hub-tip ratio. The mode shape is independent of the duct flow Mach number. c_{mn} is the modal amplitude.

A spinning mode of order m and frequency ω will propagate through the duct only if its cut-off ratio is greater than or equal to unity. The cut-off ratio is defined as

$$\xi = \frac{(\omega/c)r_o}{k_{mn}\sqrt{1-M_d^2}} \quad (2)$$

where M_d is duct Mach number, ω is frequency, k_{mn} is mode eigen value, r_o is duct radius and c is speed of sound. If the cut-off ratio is less than unity, the mode decays rapidly or is "cut-off". Stated differently, the circumferential Mach number of the pressure pattern at the outer wall, $(\omega r_o/m)/c$ should be greater than unity for a mode to propagate. Then, how does a subsonic rotor produce blade passing tone and its harmonics? It was first explained by Tyler and Sofrin in terms of the interaction of rotor-stator fields. If the rotor in a fan stage contains B rotor blades and the stator contains V vanes, the interaction will set up circumferential modes of order m given by $m = sB - kV$. s is the harmonic of the blade passing frequency (BPF) tone and k is an integer. The speed of rotation of mode m is (sB/m) times rotor speed. If m is small, the speed of the interaction mode will be supersonic and above cut-off. By proper choice of the number of blades and vanes, the BPF and one or more of its harmonics may be cut-off, reducing the noise generated.

Inlet Radiation

Eversman and Roy (ref. 2) solve the radiation problem by a finite element method. The propagation in the duct and the radiation to the far-field are included in one model. The inlet flow is assumed to be irrotational. The acoustic problem is formulated in terms of the acoustic perturbation velocity potential. They solve the duct eigen value problem for the duct with uniform flow. The equation turns out to be a Bessel's equation of order m . The finite element solution of this equation is the approximation to the exact solution given by expression (1). They employ a Galerkin type finite element formulation with isoparametric elements. The mean flow is computed using a velocity potential formulation, on the same mesh as that used for acoustic propagation and radiation. The acoustic field equations are written in terms of the acoustic potential and acoustic pressure and solved using finite element techniques.

The source is modeled in terms of the incident and reflected modes which are matched to the finite element solution on the same plane. Wave envelope elements are used in the far-field, assuming that the sound field there approximates that produced by a point source. It is assumed that only outgoing waves exist at the far-field boundary. A Sommerfeld radiation condition for a monopole in a uniform flow is applied there. The same boundary conditions are applied at the baffle boundary (fig. 1). With the wave envelop elements in the far-field the entire radiation field can be modeled with a relatively small number of finite elements. The solution to the finite element system is obtained using a frontal solution method. Further details of the finite element formulation and the solution procedure may be found in (ref. 2).

Aft Radiation

The equations governing the acoustic field of the aft radiation are the same as that of the inlet. However, the jet shear layer introduces complication for the computation of the mean flow. The shear layer is modeled as though the duct is extended four duct radii beyond the exit plane (ref. 3). The velocity potential is allowed to be discontinuous across the shear layer. The acoustic pressure is continuous over the entire region. Beyond this "extended" duct, the internal and external flows are allowed to mix and the velocity potential is continuous everywhere. The extent of the "extended" duct can be varied if needed. Other boundary conditions are treated in the same way as in the inlet radiation code.

Duct Lining

One of the fan noise suppression techniques is to line the duct walls with materials of appropriate surface impedance to absorb part of the generated fan noise. The finite element technique developed by Eversman and Roy can handle lined surface by specification of the impedance of the treated elements. The impedance z , is equal to $p/v.n$, where p is the acoustic pressure and $v.n$ is the normal component of the lining velocity at the wall. z is normalized with respect to $(\rho c)_{\infty}$. The lined element is defined in terms of its normalized impedance

$$z = R + i X \quad (3)$$

where R is the normalized resistance and X is the normalized reactance. Lining optimization methods are employed to obtain the optimum impedance for maximum attenuation (ref. 3).

Geometry and Computational Domain

The parametric study was done on Active Noise Control (ANC) fan that is being tested in the Aeroacoustic Propulsion Laboratory which is the anechoic dome acoustic facility at Lewis Research Center. A sketch of the inlet geometry and the computational domain are shown in figure 1. The computational domain has regions labeled duct region and far-field region and the acoustic pressure distributions in these regions will be presented and discussed below. Figure 2 shows a sketch of the aft duct geometry and the computational domain. The far-field boundary is located at 20 radii where far-field measurements are made. A long center body and a flanged exit characterize the aft duct geometry. The effect of the flange and the aft center body will be discussed in the results section. For the purpose of the parametric study the source (input) plane is chosen as the rotor pitch change axis (fan face) and a unit amplitude is used as the input. The propagation through the inlet and aft ducts and the respective far-field radiation are studied.

The rotor has 16 blades and the number of vanes can be varied in the tests to study different aspects of the radiation characteristics. However, for the present study, a 14 vane stator is used resulting in the following propagating modes at the design speed.

Harmonics (s)	Modes (m,n)	Cut-off ratio	
		Inlet	Aft
1BPF	(2,0)	1.91	2.11
2BPF	(4,0)	2.13	2.19
	(4,1)	1.24	1.28
3BPF	(6, 0)	2.26	2.28
	(6, 1)	1.45	1.51
	(6, 2)	1.12	1.11
	(-8, 0)	1.76	1.77
	(-8, 1)	1.21	1.23

The propagation characteristics of these modes in the ducts and the radiation to the far-field are examined. The fan radius is 2 ft and design speed is 1886 rpm. The fan face Mach number is 0.1 and there is no external flow.

Typical finite element grids employed for the inlet and the aft are shown in figures 3 and 4 respectively. The inlet grid had 2765 eight node isoparametric finite elements with 875 elements in the duct region. The aft grid had 3466 elements with 660 elements in the duct region. These grids were found to give adequate resolution to compute up to the third harmonic of the blade passing frequency tone. Details of the grid requirements and the distributions and inputs required to generate them are discussed in (refs. 5 and 6).

RESULTS AND DISCUSSIONS

The results of the parametric study of the inlet and aft radiation patterns of the ANC fan are presented and discussed. The input modal amplitude is specified as unity in the study to obtain the general picture of the radiation patterns. At any circumferential mode order m , the radial order mode shapes are given by the Bessel functions (of the first and second kind) as described above, equation (1). Figure 5 shows the first three radial order ($n=0,1,2$) mode shapes for a circumferential mode order $m=6$. As shown in the figure, the maximum value of each radial order is normalized to unity for computational convenience. The inlet and aft far-field radiation patterns for the three radial modes are shown in figure 6. In either case, the zero order radial mode dominates and successively higher order radial modes fall off and the lobes move away from the axis. The far-field angle is measured with respect to the inlet axis. Far-field shape measurements by Cumptsy (ref. 7) show similar behavior of different radial orders at low speed. Thus the qualitative features of the computed far-field shapes are consistent with the experimental observations.

Next, a more detailed picture of the pressure distribution in the duct as well as far-field region is presented. The pressure distributions in the inlet duct for three circumferential mode orders, $m = 2, 4$, and 6 at first radial order $n = 0$ are shown in figure 7. It is seen that the waves propagate through the duct essentially unattenuated except for small changes in the exit plane. The pressure distributions in the far-field region for the same mode orders are shown in figure 8. The principal lobe size decreases with increase in harmonic number as would be expected. This fact is brought out clearly from the far-field directivity plots in figure 9. The far-field directivities are also shown for higher order radial modes, $(4,1)$, $(6,1)$ and $(6,2)$. For the radial order $n = 1$, one side lobe develops while for $n = 2$ two side lobes appear. The principal lobe becomes smaller in size with increase in radial order.

Aft duct pressure distributions are shown in figure 10 for circumferential mode orders, $m = 2, 4$, and 6 . The aft duct with changing cross sectional area, flanged exit and long center body influence the pressure distribution in the duct, particularly at the low m order, mode $m = 2$. The radial pressure profile at a microphone plane (-0.075 from the exit) deviates significantly from Bessel function type profile. That is, the maximum pressure occurs in the duct rather than near the wall for $(2,0)$ mode. The measurements show similar profile with off the wall maximum for this mode. (Computations show that such profiles occur for m orders up to 3). The pressure distributions for the three modes in the far-field are shown in figure 11. The far-field directivities including those for higher radial mode orders ($n = 1, 2$) for 2BPF and 3BPF, are shown in figure 12. It is seen that modes $(4,0)$ and $(6,0)$ develop side lobes (away from the aft axis) the one for $(6,0)$ being more pronounced. This appears to stem from the exit flange and is absent in the inlet directivities (fig. 9). However, the side lobes equal to the number of the radial order appearing near the axis observed at the inlet appear also in the aft far-field directivities, but are far less pronounced.

A composite picture of the far-field directivity from 0 to 180 degrees, combining the inlet and aft radiation results is shown in figure 13(a) for the BPF. In the intermediate region where the radiation from the inlet and aft interfere with each other, the mean square pressures from the inlet and aft have been added to get the resultant curve. It is thus possible to compute the entire far-field directivity using the present inlet and aft radiation codes. Such computations have been made and compared with the measurements and will be reported elsewhere. The acoustic pressure contours in the entire far-field region of the inlet and aft ducts are shown in figure 13(b).

Far-field Principal Lobe Angle

Rice et al. (ref. 8) studied the relation between the propagation angle in the duct and the far-field radiation. The angle made by the normal to the local wave-front with the coordinate axes is defined as the mode propagation angle. They found that the mode propagation angle in the duct closely approximates the angle of the principal lobe of the far-field radiation. The far-field lobe angle was obtained using the Wiener-Hopf technique. The expression for the principal lobe angle for no flow is given by

$$\cos \psi_p = \sqrt{1 - \xi^2} \quad (4)$$

ξ is the cut-off ratio of the (m,n) mode.

When the duct Mach number is zero, the equation for the principal lobe angle applies to the aft duct as well.

The radiative directivity patterns of acoustic modes in an unflanged circular duct with and without uniform flow in the duct was presented by Homicz and Lordi (ref. 9). The expression for the principal lobe angle when there is a uniform flow in the duct is given by Homicz and Lordi as

$$\cos \psi_p = \beta \sqrt{\frac{(1 - \zeta^2)}{[1 - M_d^2(1 - \zeta^2)]}} \quad (5)$$

where

$$\zeta = \frac{k_{nm}}{[(\omega/c)/\beta]}$$

and

$$\beta = \sqrt{1 - M_d^2}$$

Radiation from the aft duct of a turbofan was analyzed by Savkar (ref. 10) allowing for the velocity and temperature mismatch between the external and duct flows. Rice and Saule (ref. 11) developed an approximate method for aft duct radiation. It has been found that their far-field radiation results (ref. 1) are in good agreement with that of Svakar. The principal lobe angle for the aft duct radiation is given by Rice and Saule as

$$\cos \psi_p = \frac{-M + \xi \sqrt{\xi^2 - 1} (1 - M_d^2)}{\xi (1 - M_d^2) (\xi + M_d \sqrt{\xi^2 - 1})} \quad (6)$$

for the case of no external flow.

For the case of no external flow (static), Eversman radiation code was run for the mode (4,0) at different cut-off ratios for a duct Mach number of zero and the far-field principal lobe angles obtained for the inlet and aft radiation are shown in figure 14. Also shown on the plot are the values of the lobe angle given by expression (4). It is seen that for cut-off ratios less than 1.2, the principal lobe angles predicted by Eversman codes differ from that of (4). This is partly due to the baffle boundary (figs. 1 and 2) location and the boundary condition employed there in the computations. With a duct flow Mach number of 0.1 (typical in the measurements), the far field lobe angle variations are shown in figure 15. (At the inlet, the flow is in a direction opposite to that of sound wave propagation). Again, for cut-off ratios close to unity the lobe angles computed from Eversman solutions differ from those obtained from expressions 5 and 6. Near cut-off, the radiation is towards the sideline and that is when the influence of the baffle boundary and the radiation condition imposed on it creeps into the solution.

The variation of the far-field principal lobe angle with duct Mach number is shown in figure 16. An increase in the duct Mach number moves the lobe angle of the inlet radiation very slightly towards the inlet axis according to expression (5) as shown in figure 16(a). The Eversman code finite element solutions also indicate that the far-field lobe angle is nearly insensitive to the duct flow Mach number. Figure 16(b) shows the far-field lobe angle variation with duct Mach number along with the curve given by expression (6) for the aft duct. The agreement between the Eversman computations and expression 6 is good. It should be noted that the expressions 4 to 6 are derived for circular ducts (no center body).

Rice (ref. 12) studied the far-field radiation pattern for single and multi-modes as a function of cut-off ratio. The main contribution is the finding that all modes with approximately the same cut-off ratio will have approximately the same far-field radiation pattern. This idea is quite useful in the design of acoustic liners. This concept is examined with the inlet and aft radiation codes by obtaining far-field radiation patterns for different mode orders at a cutoff ratio of 1.5. Figure 17 shows the far-field lobe pattern for the inlet radiation for modes (2,0), (4,1), (6,2), and (-8,0), and the principal lobe angle for all the modes is about 43 degrees. The aft radiation patterns for the same four modes are shown in figure 18 and it is seen that the far-field lobe angle for these modes is approximately 130 degrees. Thus the inlet and aft radiation codes are able to produce far-field radiation patterns consistent with the theory.

Groeneweg and Rice (ref. 1) made an important observation that the inlet quadrant contains the near cut-off mode peaks irrespective of where the sound originated, inlet or aft. This can be easily seen from the expressions (5) and (6). Figure 19 shows the inlet (19(a)) and aft (19(b)) far field radiation patterns for a near cutoff mode, (4,0). It is seen that the principal lobe angle in either case is in the inlet quadrant. The duct Mach number for this case was -0.4 for the inlet duct and 0.4 for the aft.

Next, the effect of aft duct exit geometry variations on the far-field directivity was examined. Three simple variations (no flange, short center body, and short center body and no flange) shown in figure 20 were considered. Figure 21 shows the far-field radiation patterns for the three cases for the (2,0) mode. The first two geometry variations, no flange and short center body, produce a maximum far-field SPL that is less than that for the base geometry by about one dB. A short center body with no flange reduces the maximum SPL by about 2.7 dB. Similar but smaller reductions in maximum SPL were observed for higher harmonics, 2 and 3 BPF (not shown).

Lined Duct

Acoustic lining of the fan inlet and aft ducts is used to reduce the noise radiated to the far-field. A method of calculating optimum liner impedance for spinning modes in circular ducts was developed by Rice (refs. 13 and 14). He discovered that the mode cut-off ratio uniquely determines the optimum impedance and maximum attenuation for a given duct Mach number and frequency. He found that maximum damping is insensitive to duct wall boundary layer thickness (ref. 14).

The Eversman radiation codes can handle the lined ducts by specifying the surface impedance of the lined elements in the finite element system. To demonstrate this capability, the code was run with specified wall impedance for the lined region of the duct. It should be noted that the results presented here are for demonstration purpose only and also no test is run on the ANC fan with acoustic lining. The impedance was chosen to be close to the optimum impedance, by extrapolation from the optimum impedance curves of Rice (ref. 13), for BPF at the inlet. For simplicity, the same impedance was used for both the inlet and aft ducts, and higher harmonics. The location of the lined sections of the ducts are shown in figure 22. In actual turbofan engine applications, the acoustically lined section is usually located in the straight portion of the duct and the lining is also used on the center body. The code handles lined elements on the nacelle as well as the center body. In the present computations, the lining in both ducts is only on the nacelle surface as shown in the figure, and starts $0.061 \times \text{radius}$ from the exit plane. The length of the lined region is $0.55 \times \text{radius}$ in the inlet duct and $0.53 \times \text{radius}$ in the aft duct. The impedance chosen is

$$z = 0.45 - i 0.40.$$

The results of the lined ducts are shown in figures 23 to 26. The pressure contours in the inlet duct for modes (2,0), (4,0), and (6,0) are shown in figure 23 and can be directly compared with the pressure contours of unlined duct in figure 7. The pressure levels in and around the lined region and also across the duct in that region are significantly altered due to the liner. The pressure near the lining is reduced appreciably. The pressure maxima which occur near the wall of the duct with no lining, are moved away from the wall towards the mid-section of the duct with lining. The far-field acoustic pressure directivities for the three modes are shown in figure 24.

The pressure contours of the aft lined duct for the same three modes are shown in figure 25 and may be compared with those of the unlined duct in figure 10. The reduction in pressure levels near the liner and the movement of the pressure maxima across the duct are seen as for the lined inlet duct. Figure 26 shows the far-field directivities for the three modes.

CONCLUDING REMARKS

Turbofan inlet and aft noise radiation characteristics were examined for a low speed fan. It is shown that the inlet and aft radiation finite element codes are capable of predicting the experimentally observed and theoretical turbofan noise characteristics. The effects of cut-off ratio, duct Mach number, and aft duct exit geometry variations on the far-field principal lobe angle were presented. The capability of the codes to handle ducts with acoustic lining was demonstrated.

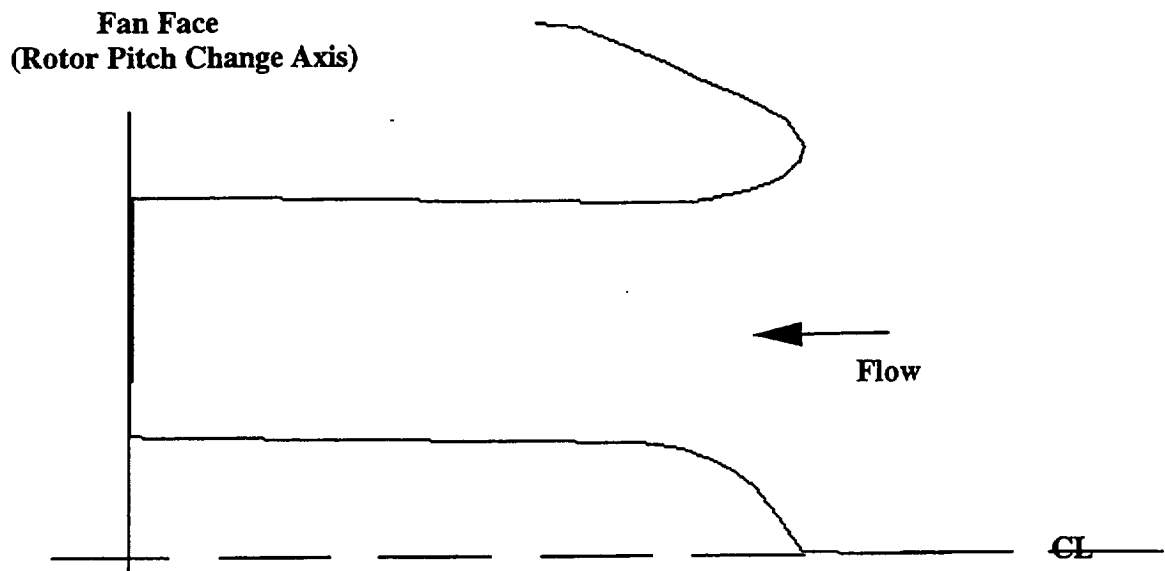
Recommendations

The baffle boundary radiation condition needs to be modified to avoid spurious reflections from this boundary contaminating the results, under some conditions. Aft radiation code needs modifications for computing high frequency cases that are more representative of modern turbofans.

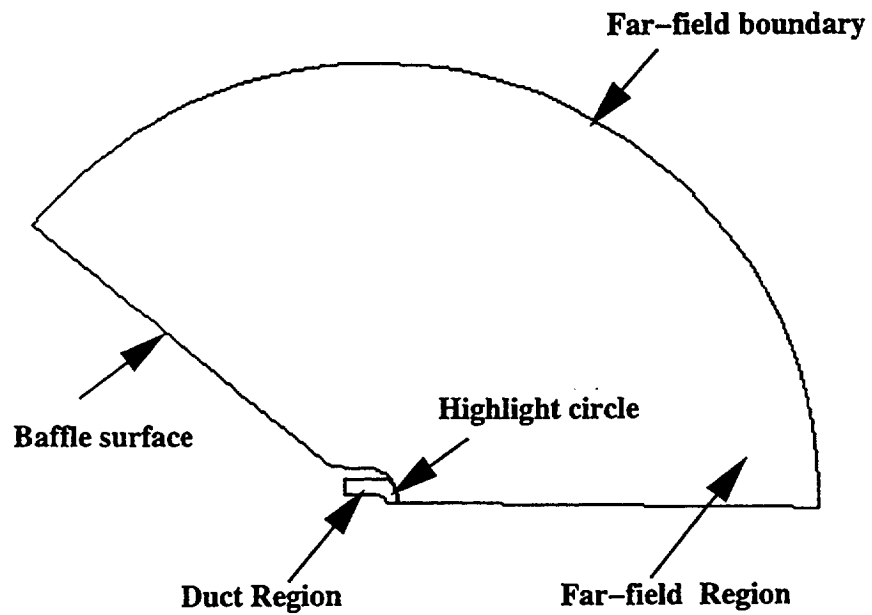
REFERENCES

1. Groeneweg, J.F.; and Rice, E.J.: Aircraft Turbofan Noise. Trans. ASME Journal of Turbomachinery, vol. 109, 1987, pp. 130-141.
2. Tyler, J.M.; and Sofrin, T.G.: Axial Flow Compressor Noise Studies. SAE Transactions, vol. 70, 1962, pp. 309-332.

3. Roy, I.D.; and Eversman, W.: Improved Finite Element Modeling of the Turbofan Engine Inlet Radiation Problem. Report for NASA contract NAS3-25952, August 1992.
4. Eversman, W.; and Roy, I.D.: Development of the Turbofan Acoustic Radiation Code: Code Improvements, Acoustic treatment, and Aft Radiation Including Shear Layer Effects. Final Report, May 1994.
5. Topol, D.A.; and Philbrick, D.A.: Fan Noise Prediction System Development: Wake Model Improvement and Code Evaluations. Report for NASA contract NAS3-25952, April 1993.
6. Topol, D.A.; and Mathews, D.C.: Rotor Wake/Stator Interaction Noise Prediction Code Technical Documentation and User's Manual. Report for NASA Contract NAS3-25952.
7. Cumpsty, N.A.: A Critical Review of Turbomachinery Noise. ASME Journal of Fluids Engineering, vol. 99, 1977, pp. 278-293.
8. Rice, E.J.; Heidmann, M.F.; and Sofrin, T.G.: Modal Propagation Angles in a Cylindrical Duct with Flow and Their Relation to Sound Radiation", NASA TM-79030, Jan. 1979.
9. Homicz, G.F.; and Lordi, J.A.: A Note on the Radiative Directivity Patterns of Duct Acoustic Modes. Journal of Sound and Vibration, vol. 41, 1975, pp. 283-290.
10. Savkar, S.D.: Radiation of Cylindrical Duct Acoustic Modes with Flow Mismatch. Journal of Sound and Vibration, vol. 42, 1975, pp. 363-386.
11. Rice, E.; and Saule, A.: Far-field Radiation of Aft Turbofan Noise. NASA TM-81506, 1980.
12. Rice, E.J.: Multimodal Far-Field Acoustic pattern Using Mode Cutoff Ratio. AIAA Journal, vol. 16, 1978, pp. 906-911.
13. Rice, E.J.: Acoustic Liner Optimum Impedance for Spinning Modes with Mode Cut-off Ratio as the Design Criteria. NASA TM-X-73411, 1976.
14. Rice, E.J.; and Sawdy, D.T.: A Theoretical Approach to Sound Propagation and Radiation for Ducts with Suppressors. NASA-TM-82612, 1981.

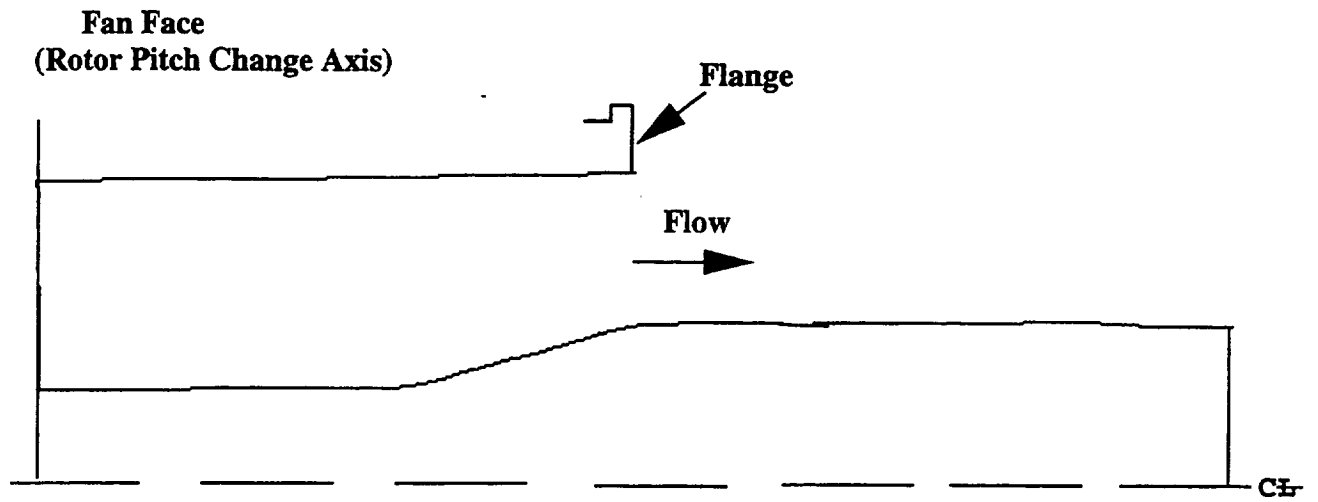


(a) Inlet Geometry

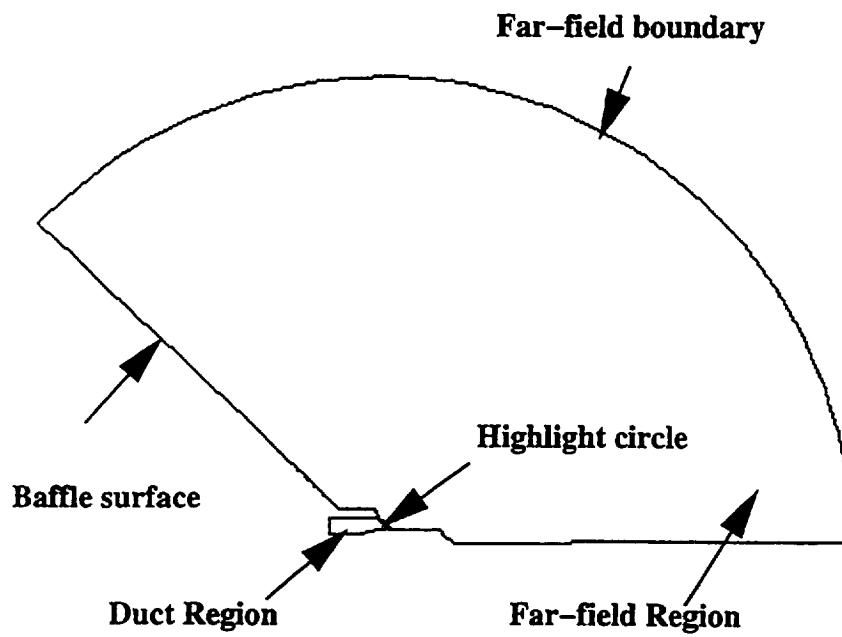


(b) Computational Domain

Fig.1 Inlet geometry sketch and computational domain



(a) Aft Geometry



(b) Computational Domain

Fig. 2 Aft geometry sketch and computational domain

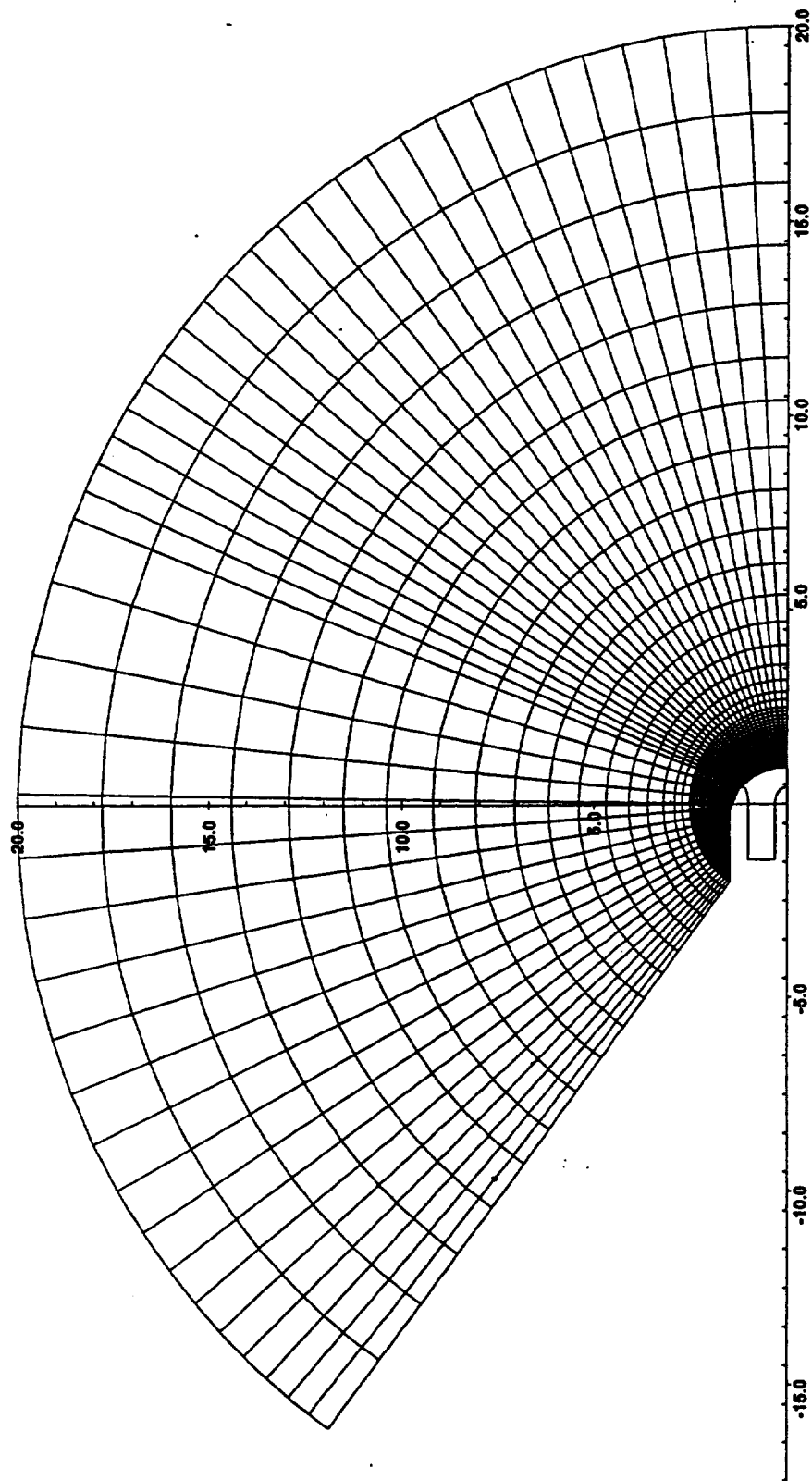


Fig. 3 Typical inlet computational grid

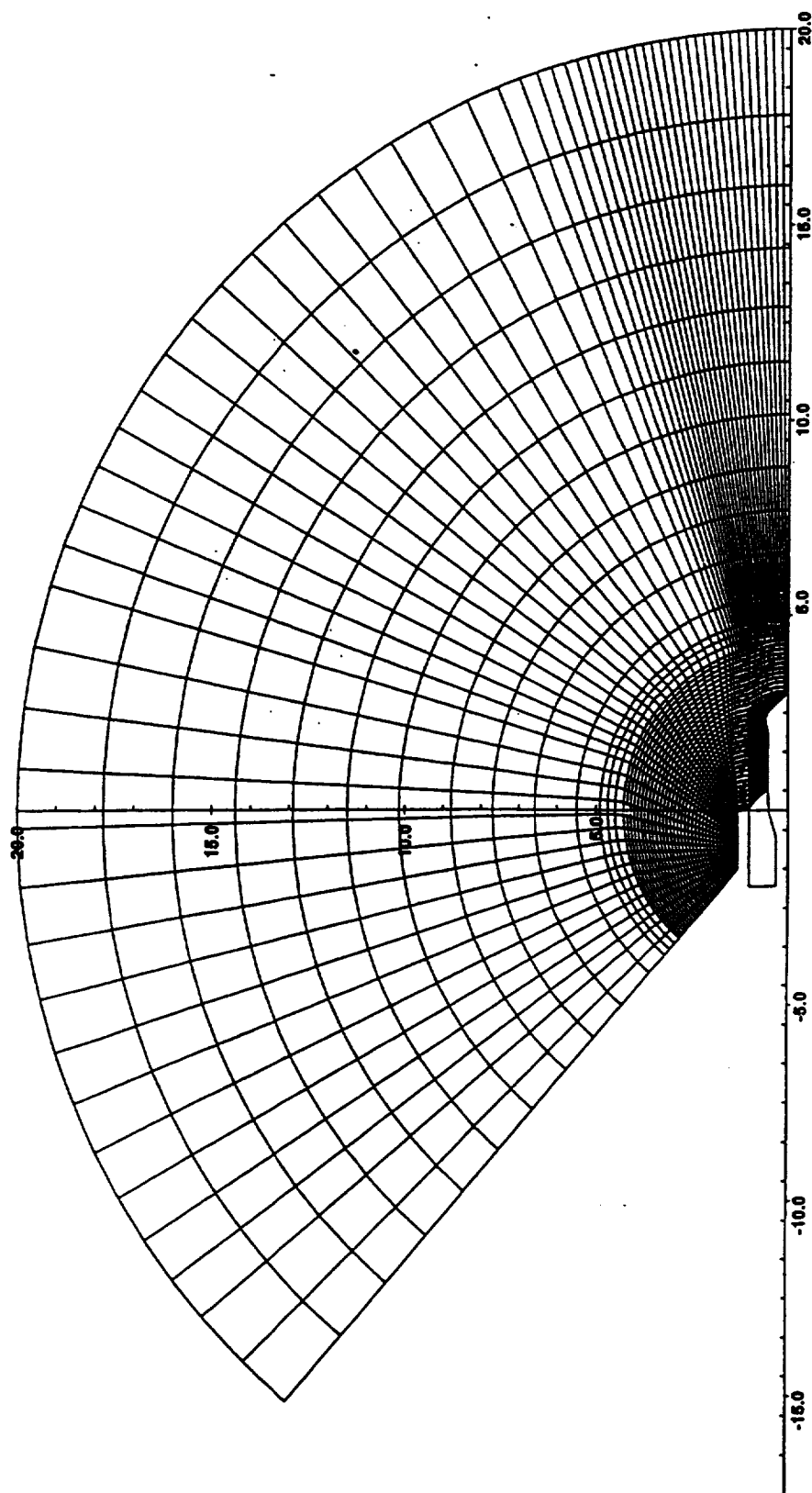


Fig. 4 Typical aft computational grid

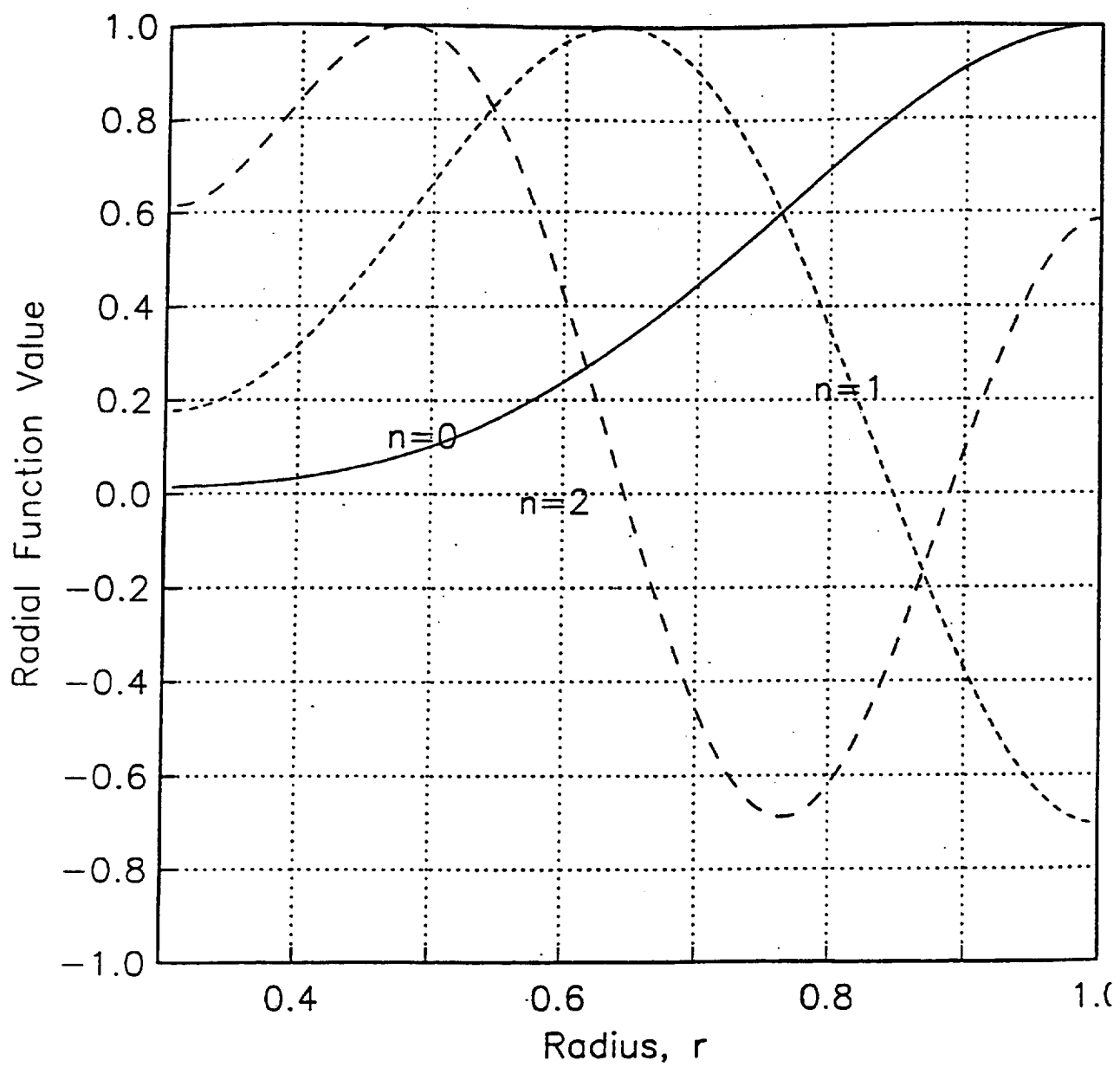


Fig. 5 Radial mode shapes, $m=6$.

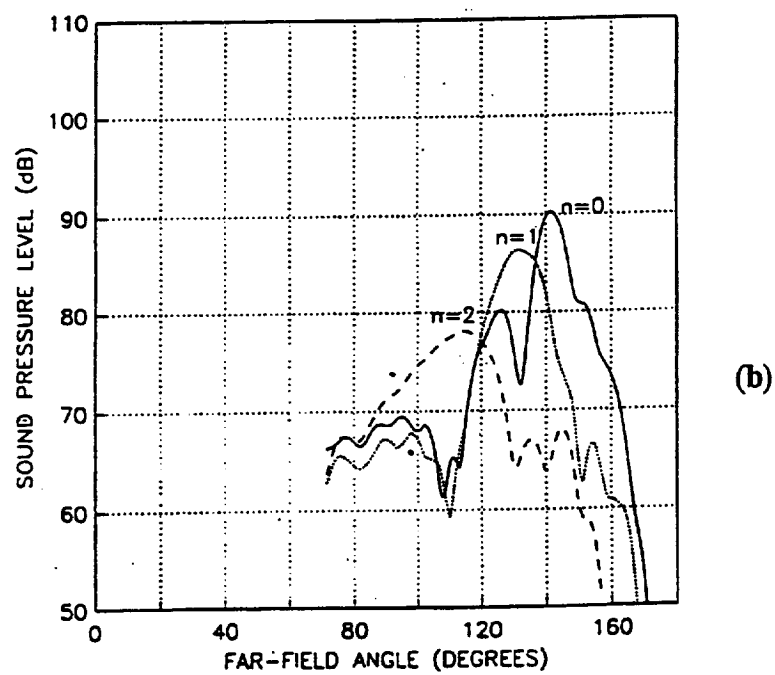
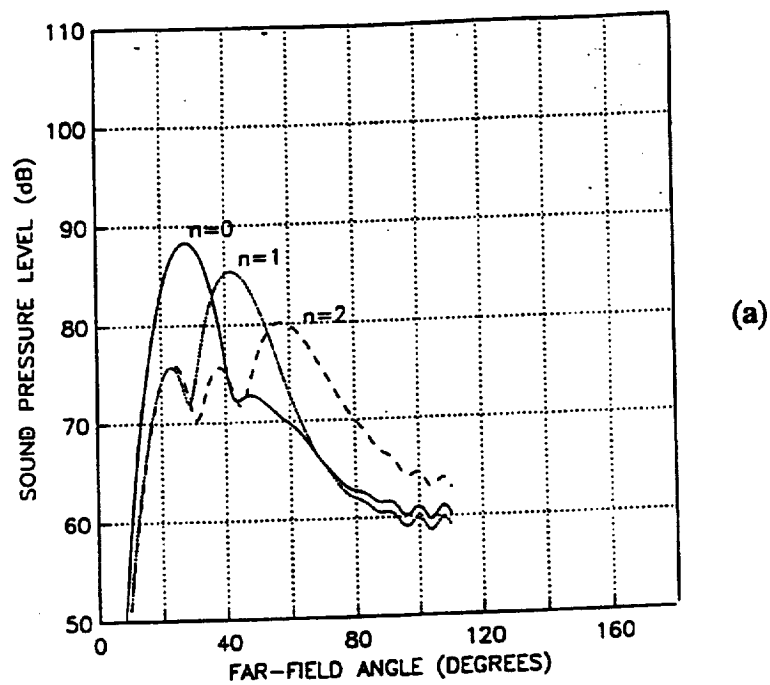


Fig. 6 Far-field shapes: (a) inlet, (b) aft.

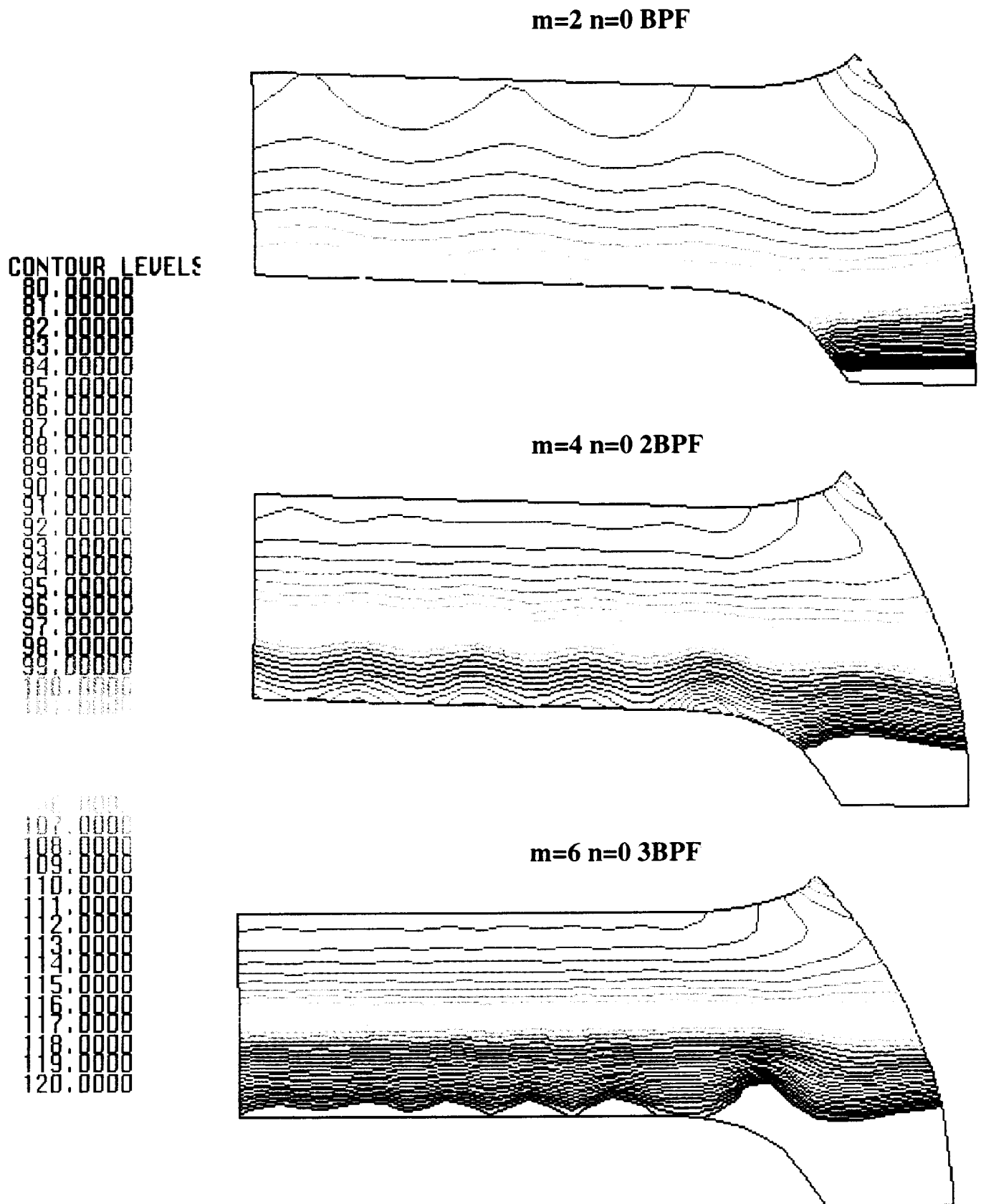
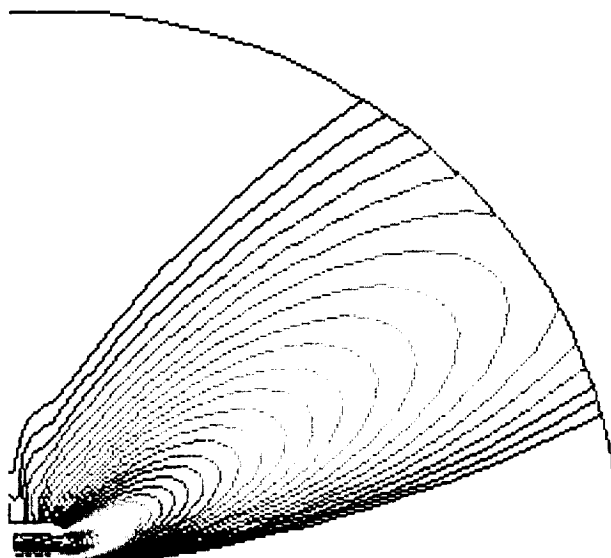


Fig. 7 ANC Fan inlet duct pressure (dB) contours 1886 rpm 16 B 14 V
Unit amplitude input at fan face

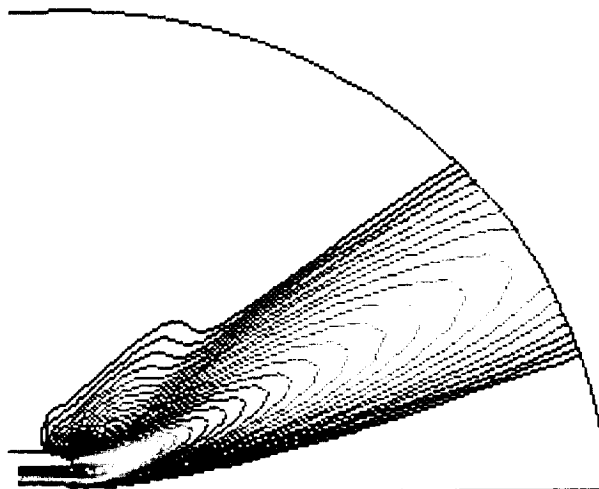
CONTOUR LEVELS

80.000000
81.000000
82.000000
83.000000
84.000000
85.000000
86.000000
87.000000
88.000000
89.000000
90.000000
91.000000
92.000000
93.000000
94.000000
95.000000
96.000000
97.000000
98.000000
99.000000
100.000000

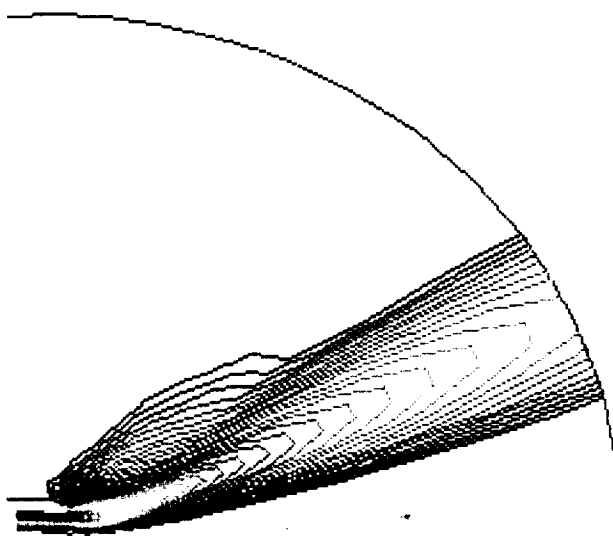
101.000000
102.000000
103.000000
104.000000
105.000000
106.000000
107.000000
108.000000
109.000000
110.000000
111.000000
112.000000
113.000000
114.000000
115.000000
116.000000
117.000000
118.000000
119.000000
120.000000



m=2 n=0



m=4 n=0



m=6 n=0

Fig. 8 ANC Fan inlet radiation levels (dB) 1886 rpm 16 B 14 V
Unit amplitude input at fan face

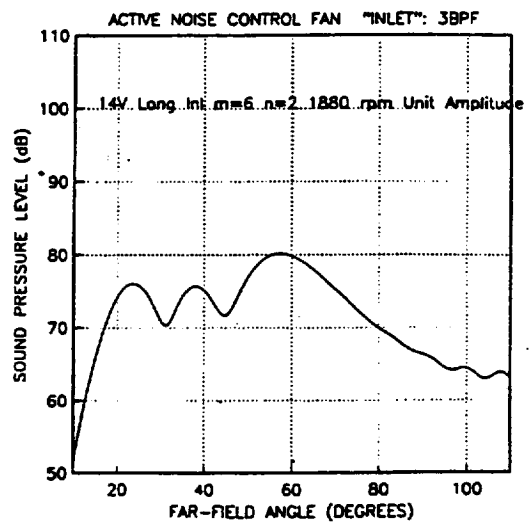
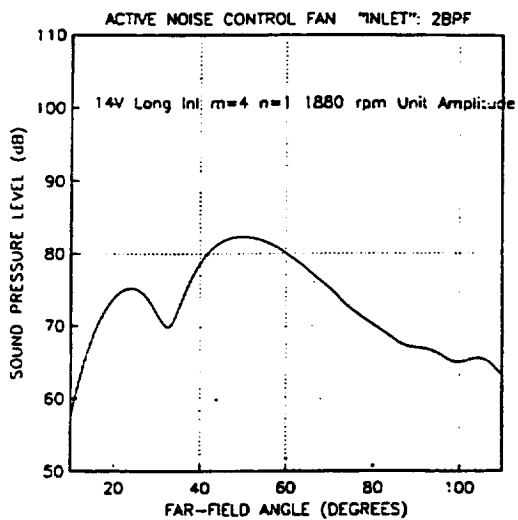
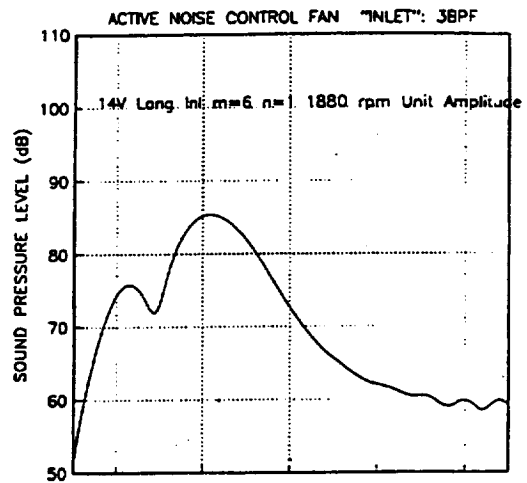
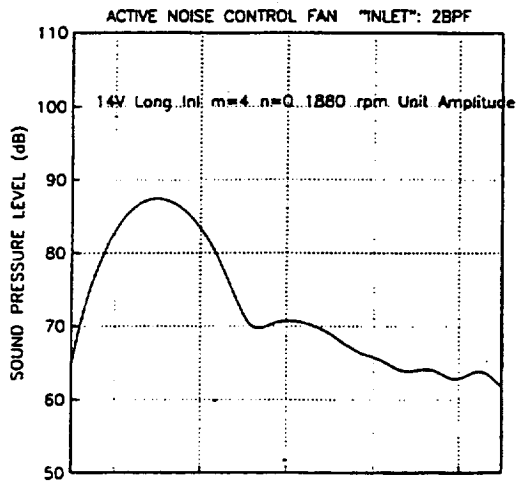
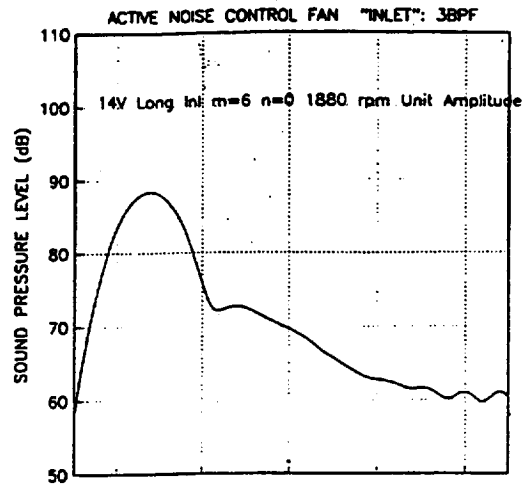
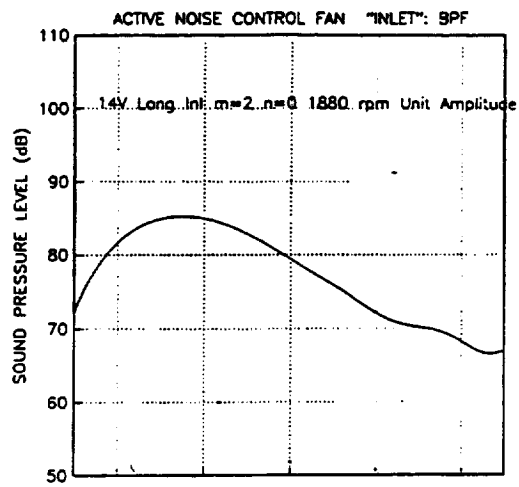
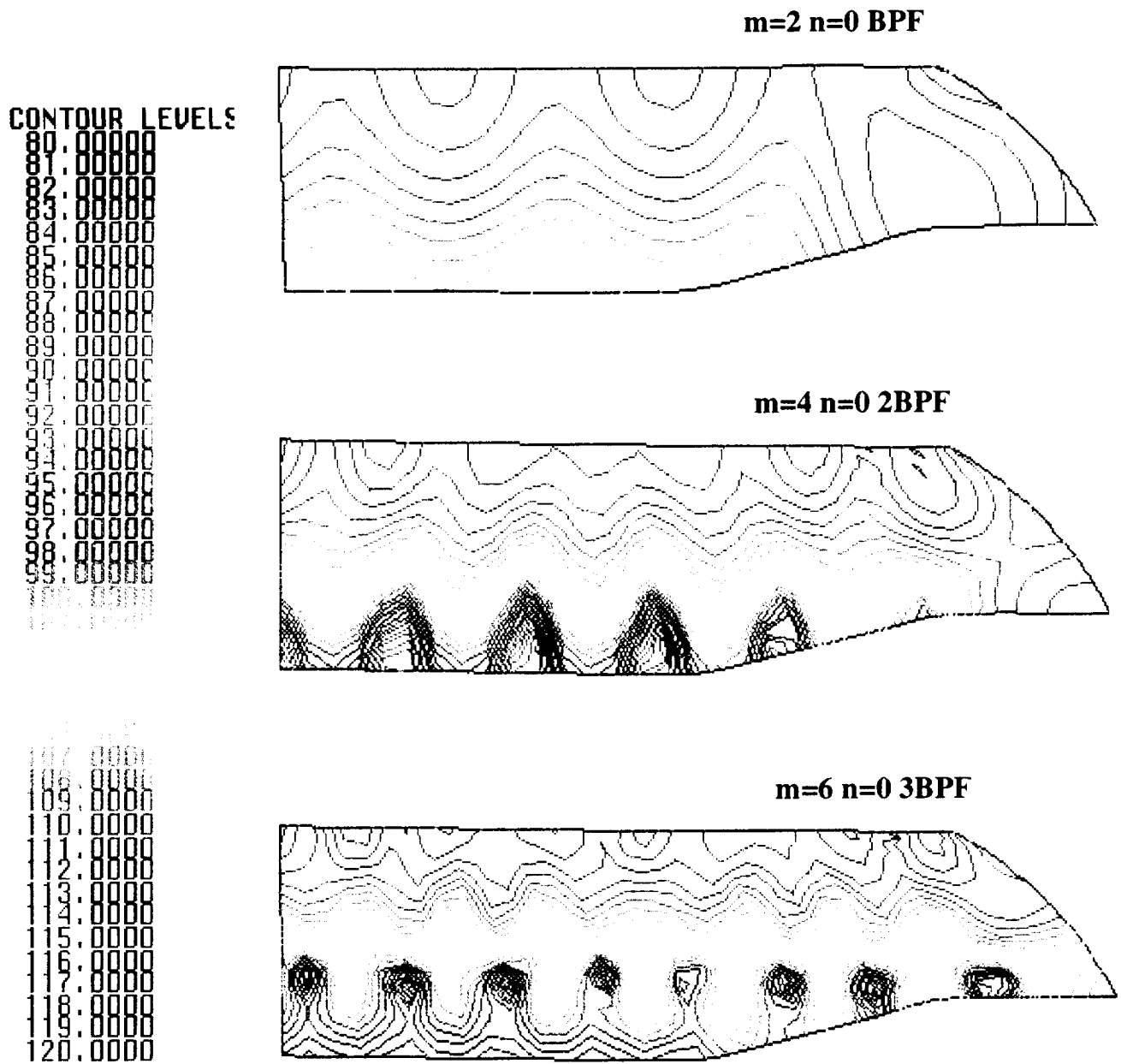


Fig. 9 Far-field directivities: Inlet



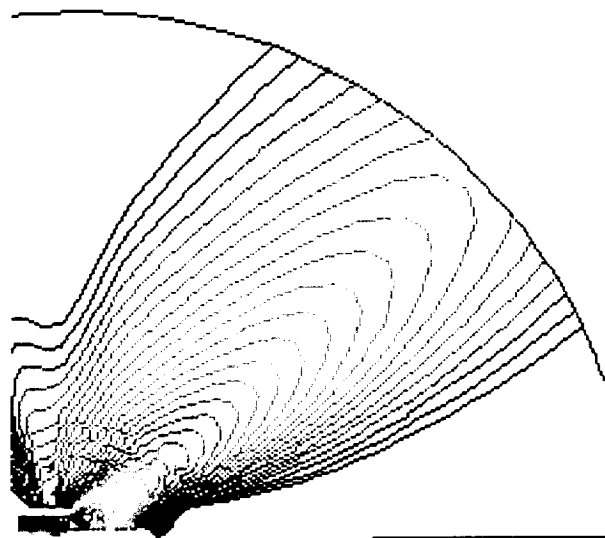
**Fig. 10 ANC Fan aft duct pressure (dB) contours 1886 rpm 16 B 14 V
Unit amplitude input at fan face**

ORIGINAL PAGE IS
OF POOR QUALITY

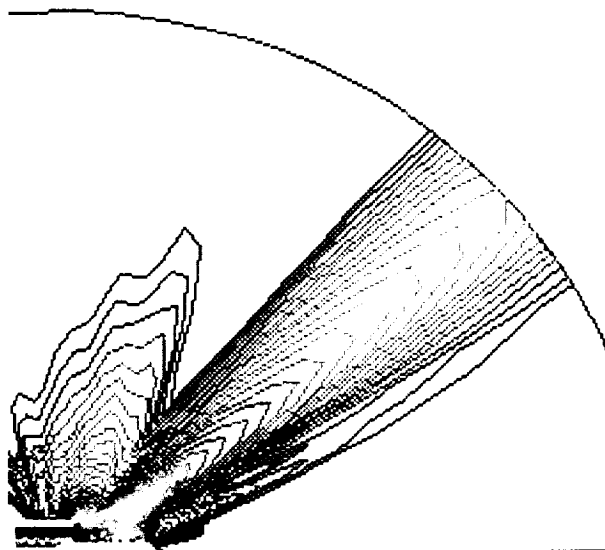
CONTOUR LEVELS

80.000000
81.000000
82.000000
83.000000
84.000000
85.000000
86.000000
87.000000
88.000000
89.000000
90.000000
91.000000
92.000000
93.000000
94.000000
95.000000
96.000000
97.000000
98.000000
99.000000
100.000000
101.000000
102.000000
103.000000
104.000000
105.000000
106.000000
107.000000
108.000000
109.000000
110.000000
111.000000
112.000000
113.000000
114.000000
115.000000
116.000000
117.000000
118.000000
119.000000
120.000000

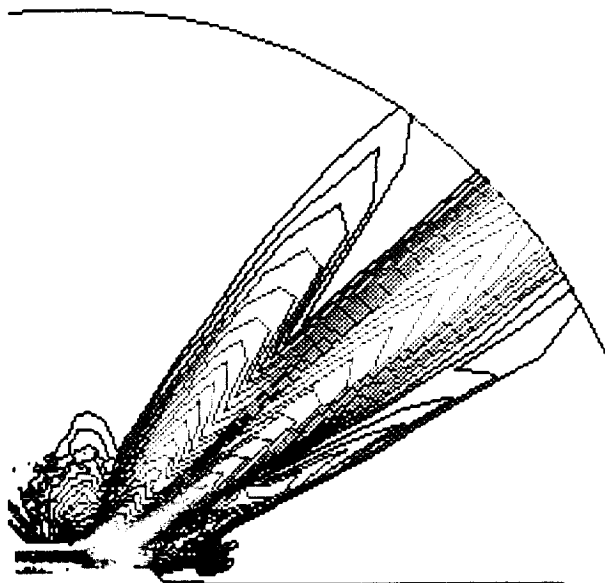
100.000000
101.000000
102.000000
103.000000
104.000000
105.000000
106.000000
107.000000
108.000000
109.000000
110.000000
111.000000
112.000000
113.000000
114.000000
115.000000
116.000000
117.000000
118.000000
119.000000
120.000000



m=2 n=0



m=4 n=0



m=6 n=0

ORIGINAL PAGE IS
OF POOR QUALITY

Fig. 11 ANC Fan aft radiation levels (dB) 1886 rpm 16 B 14 V
Unit amplitude input at fan face

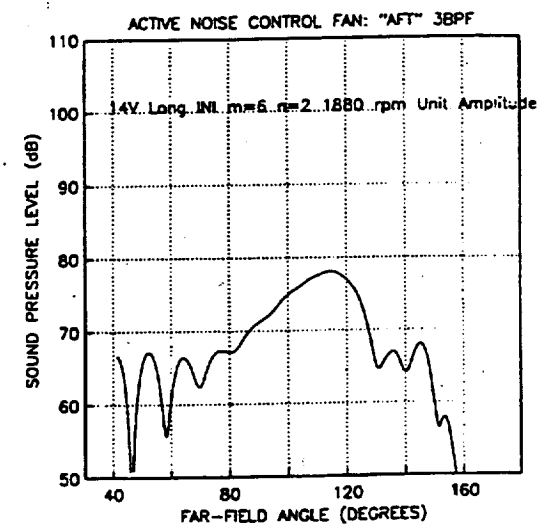
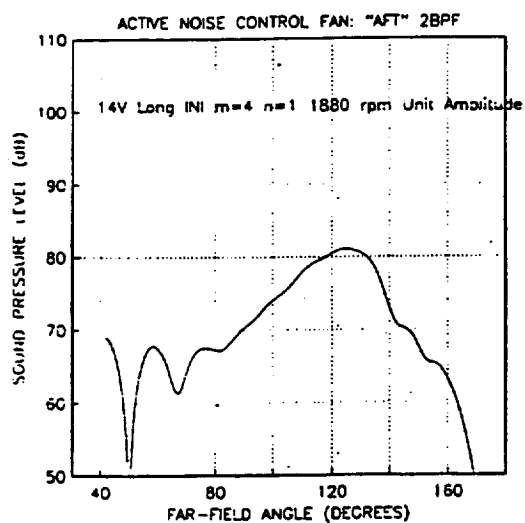
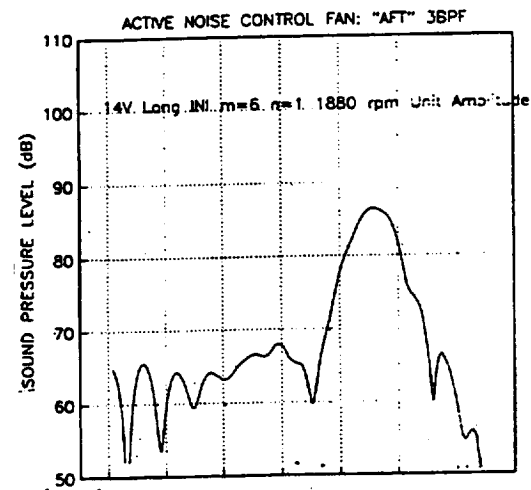
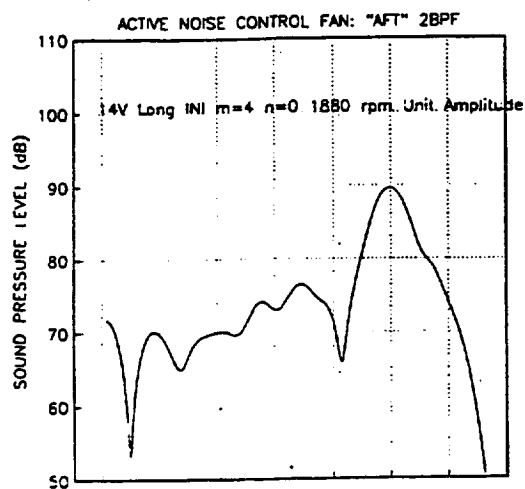
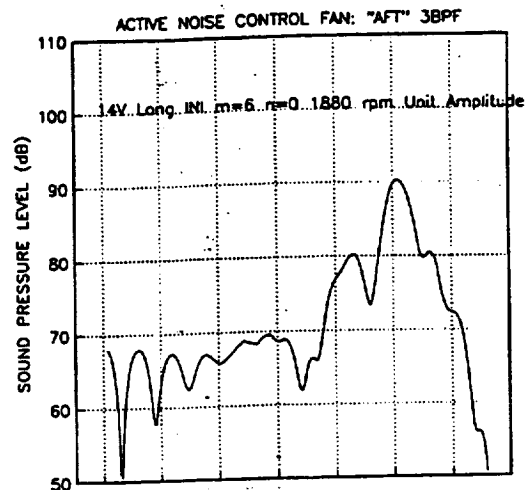
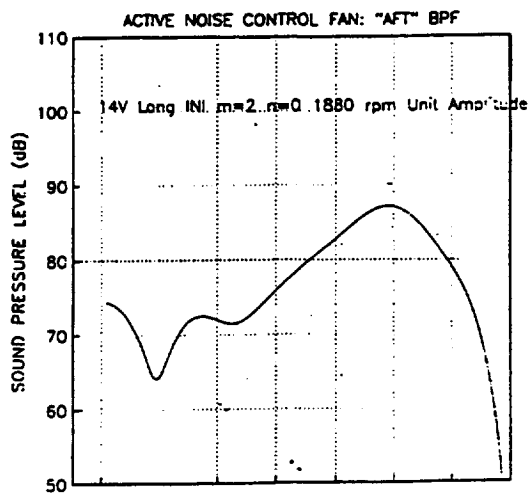


Fig. 12 Far-field directivities: Aft

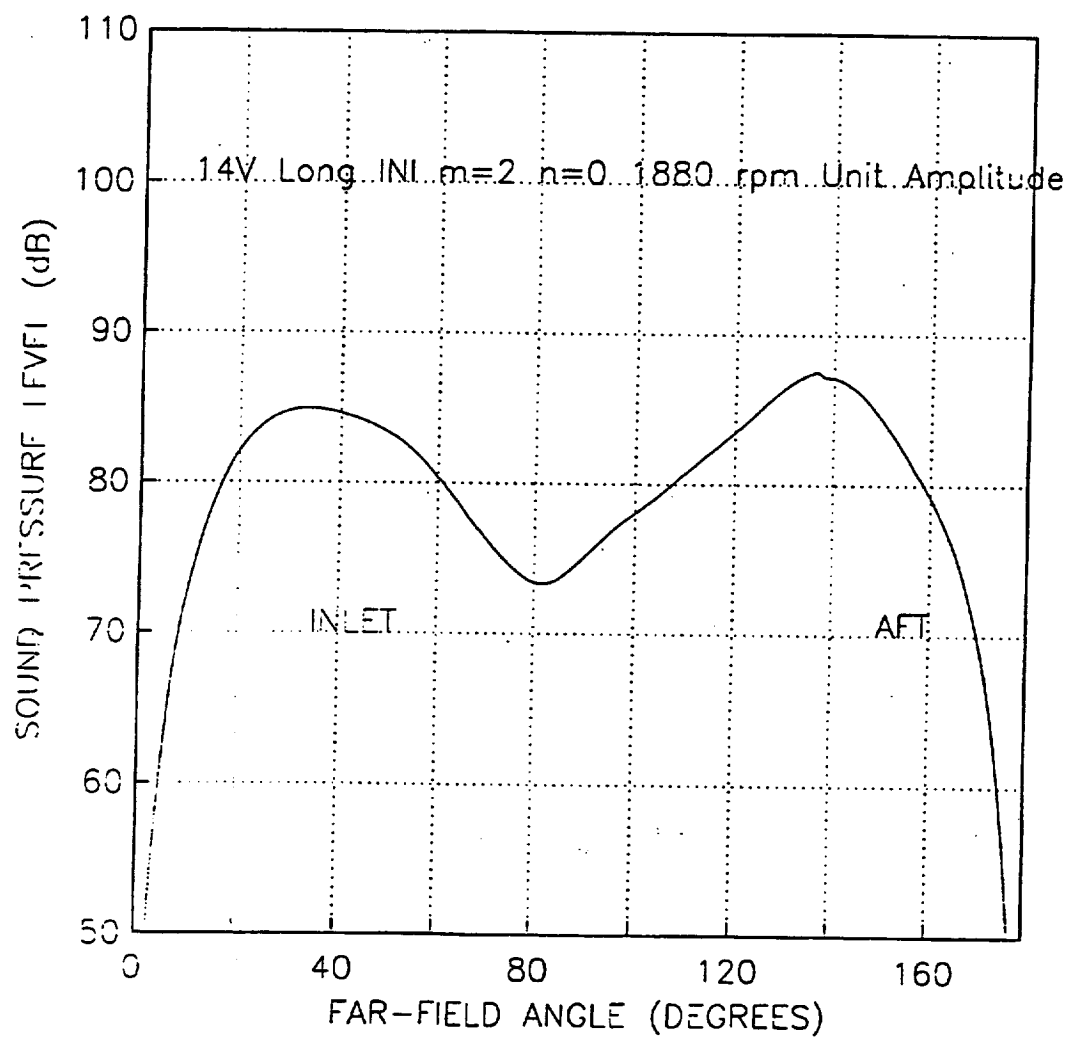


Fig. 13a Far-field BPF directivity: Inlet and Aft

CONTOUR LEVELS

80.0000
81.0000
82.0000
83.0000
84.0000
85.0000
86.0000
87.0000
88.0000
89.0000
90.0000
91.0000
92.0000
93.0000
94.0000
95.0000
96.0000
97.0000
98.0000
99.0000

107.0000
108.0000
109.0000
110.0000
111.0000
112.0000
113.0000
114.0000
115.0000
116.0000
117.0000
118.0000
119.0000
120.0000

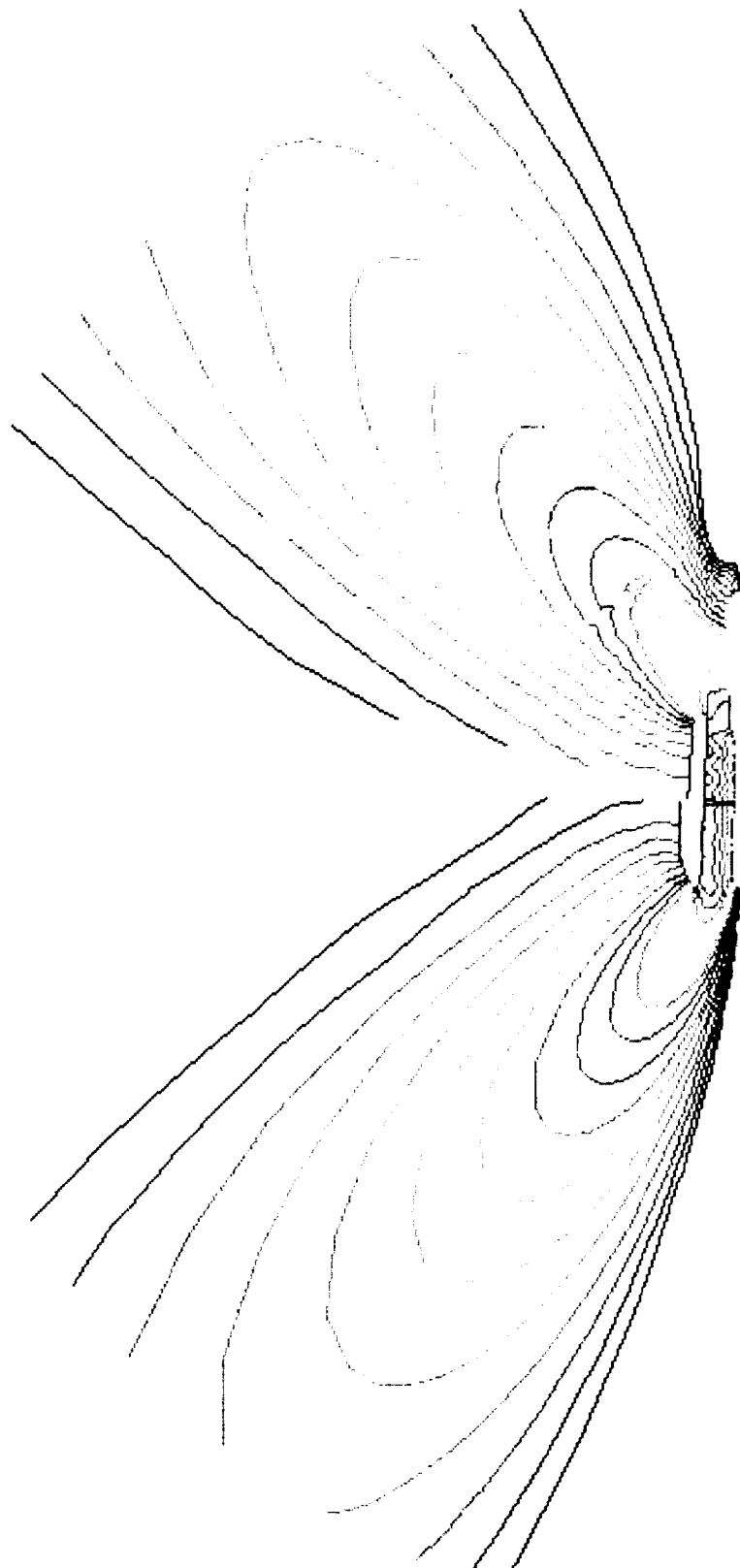


Fig. 13b ANC Fan acoustic pressure (dB) contours: 16 B 14 V 1886 rpm : BPF

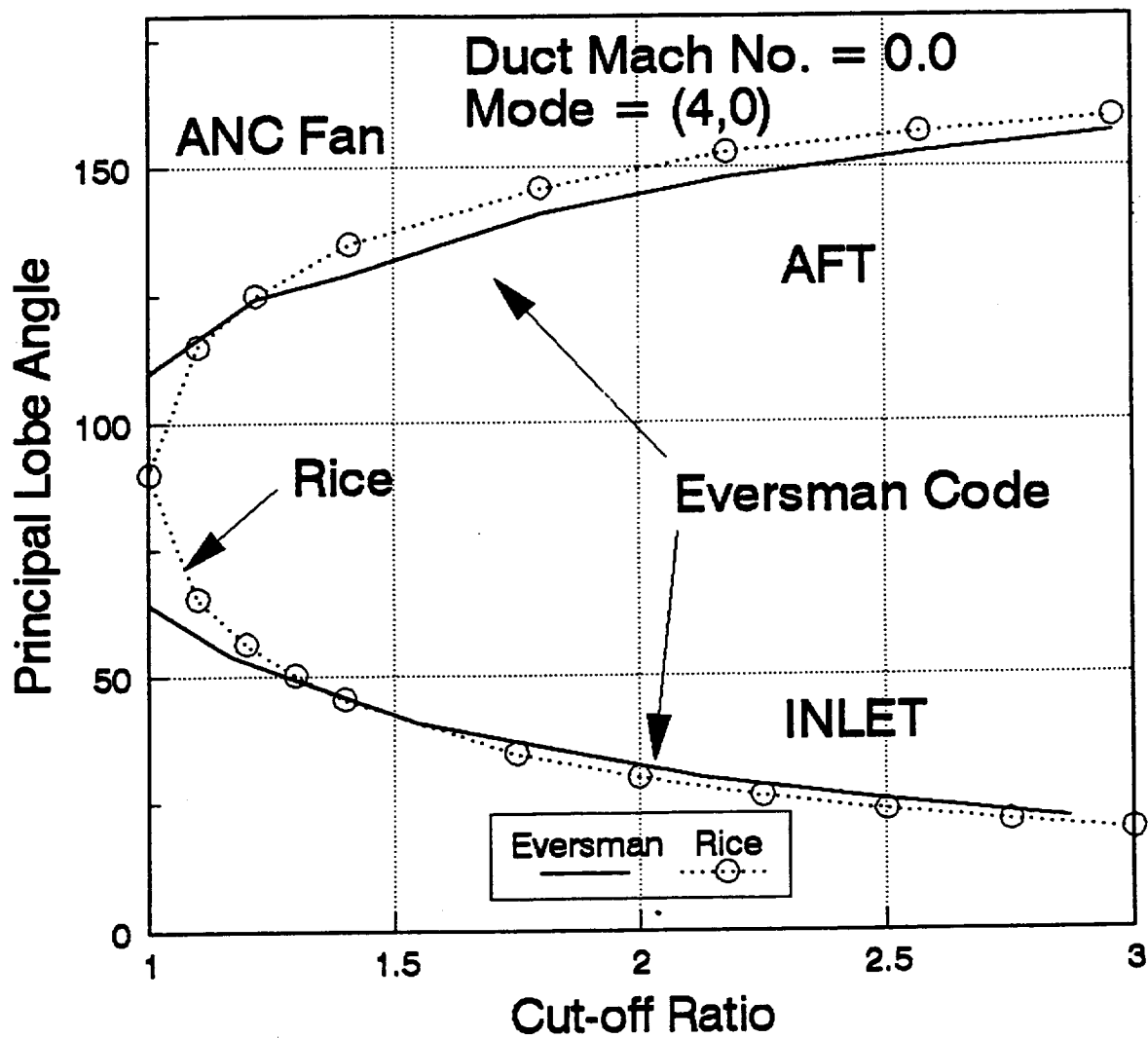
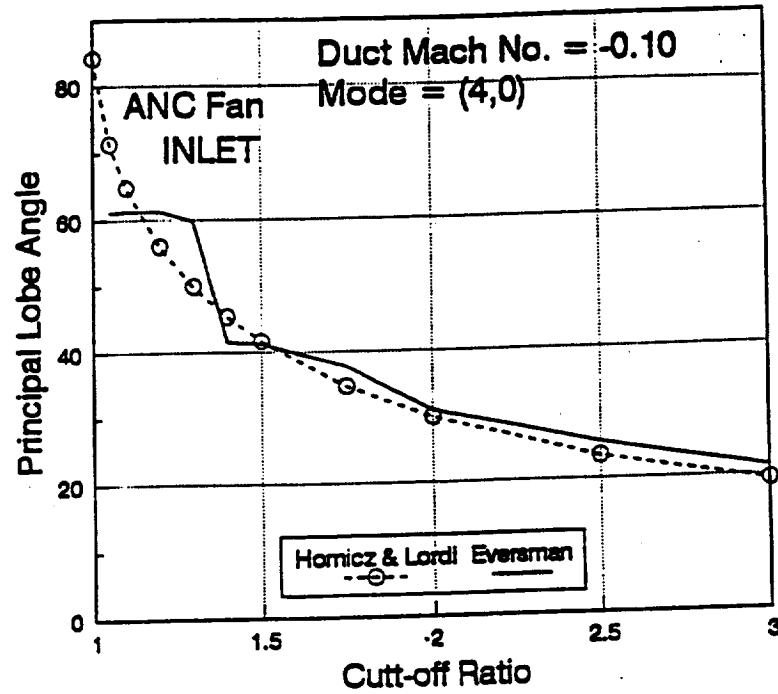
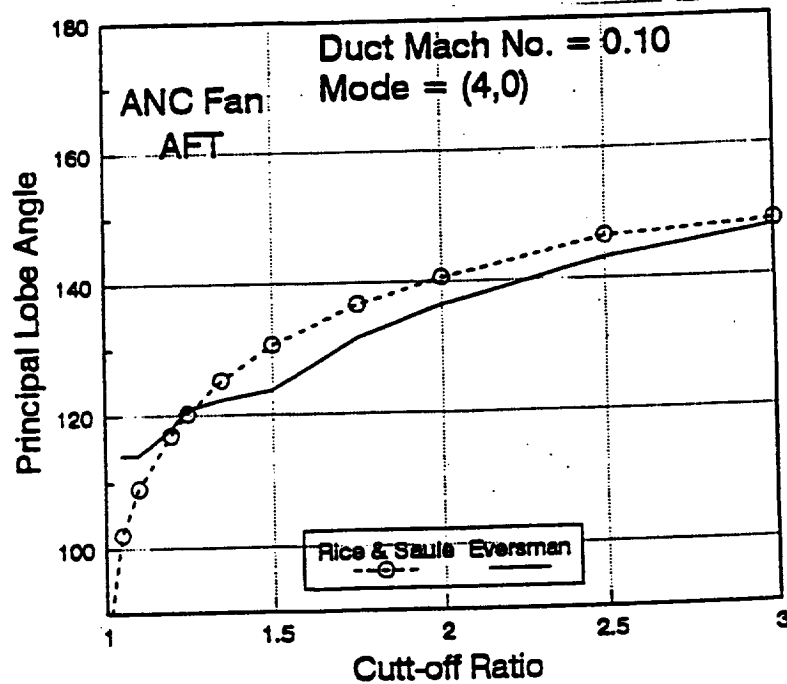


Fig. 14 Principal lobe angle variation with cut-off ratio
External flow Mach no. = 0.0

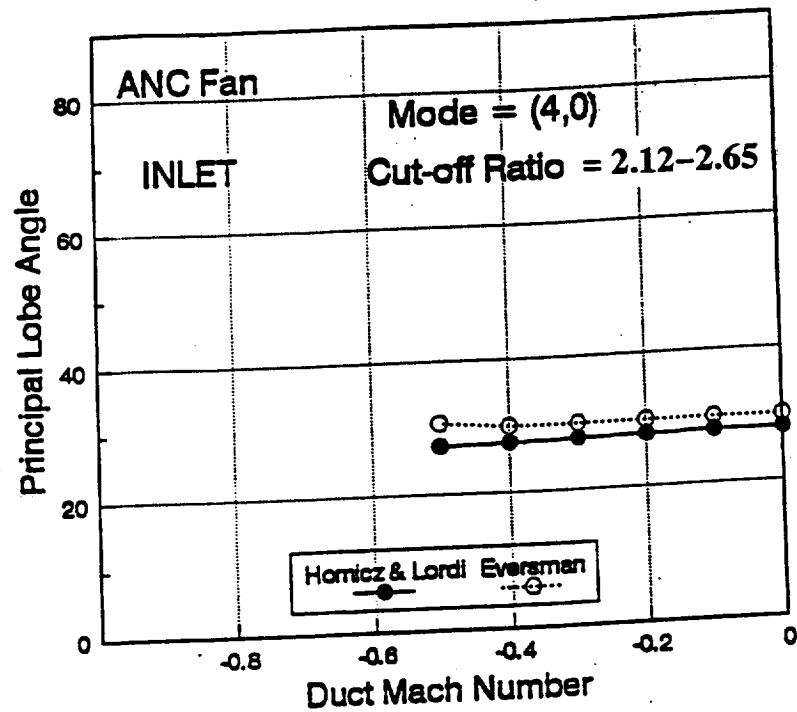


(a)

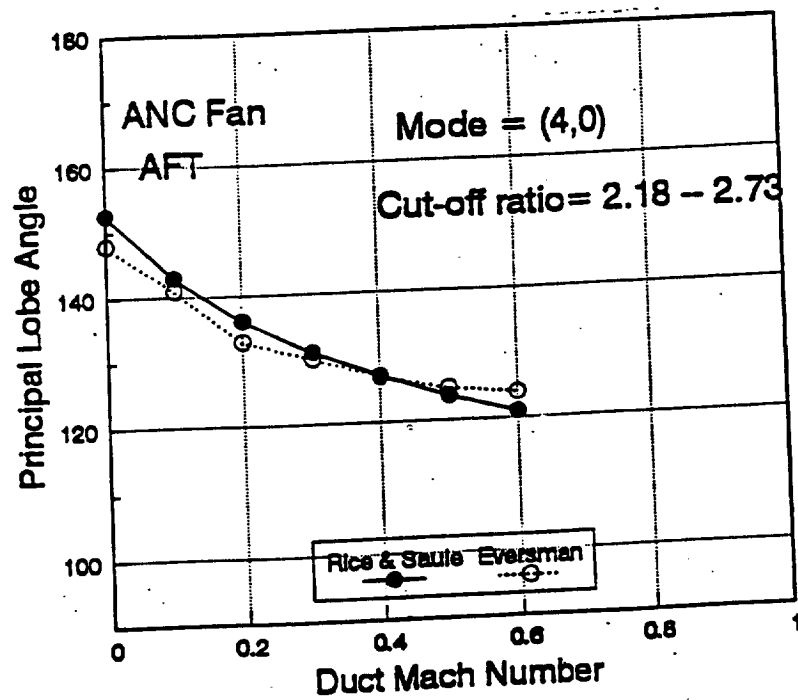


(b)

Fig. 15 Principal lobe angle variation with cut-off ratio, (a) Inlet, (b) Aft
External flow Mach no. = 0.0



(a)



(b)

Fig. 16 Principal lobe angle variation with duct Mach No., (a) Inlet, (b) Aft
External flow Mach no. = 0.0,

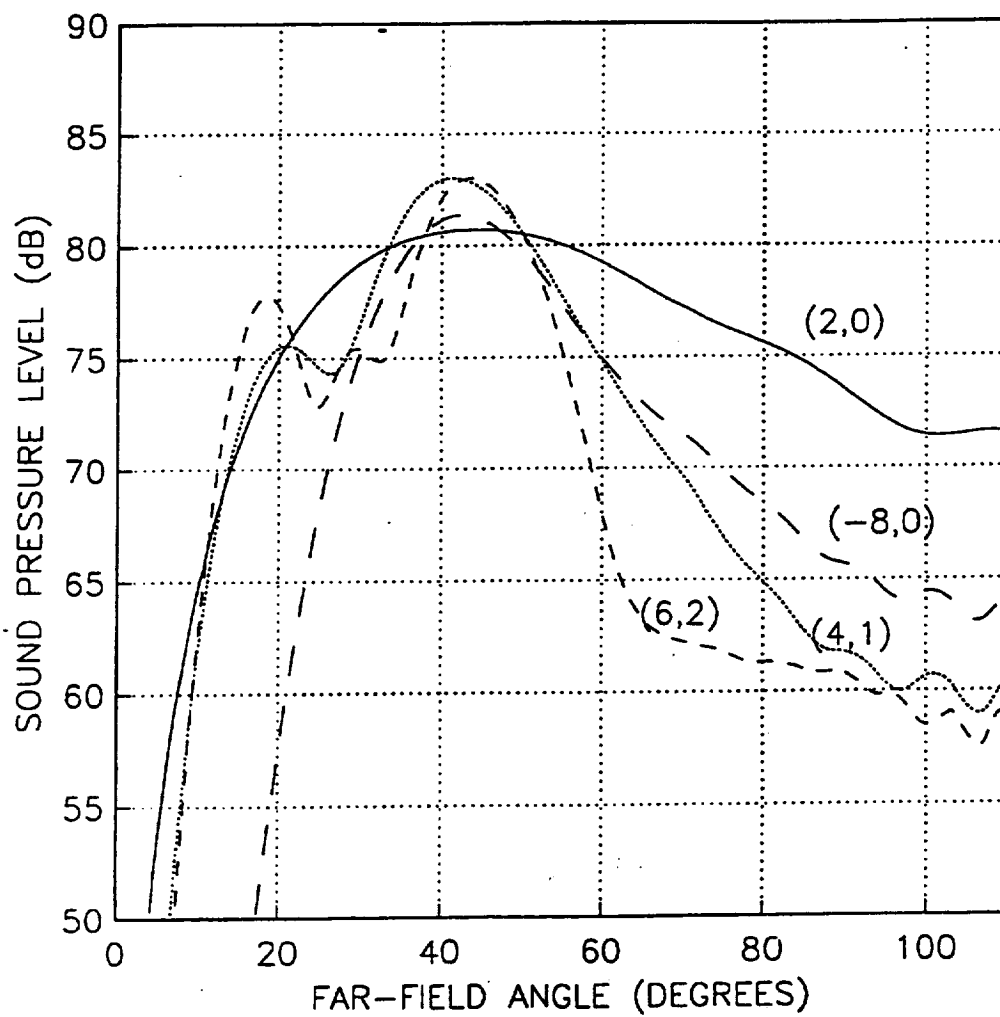


Fig. 17 Far-field shapes at a cut-off ratio of 1.5: Inlet

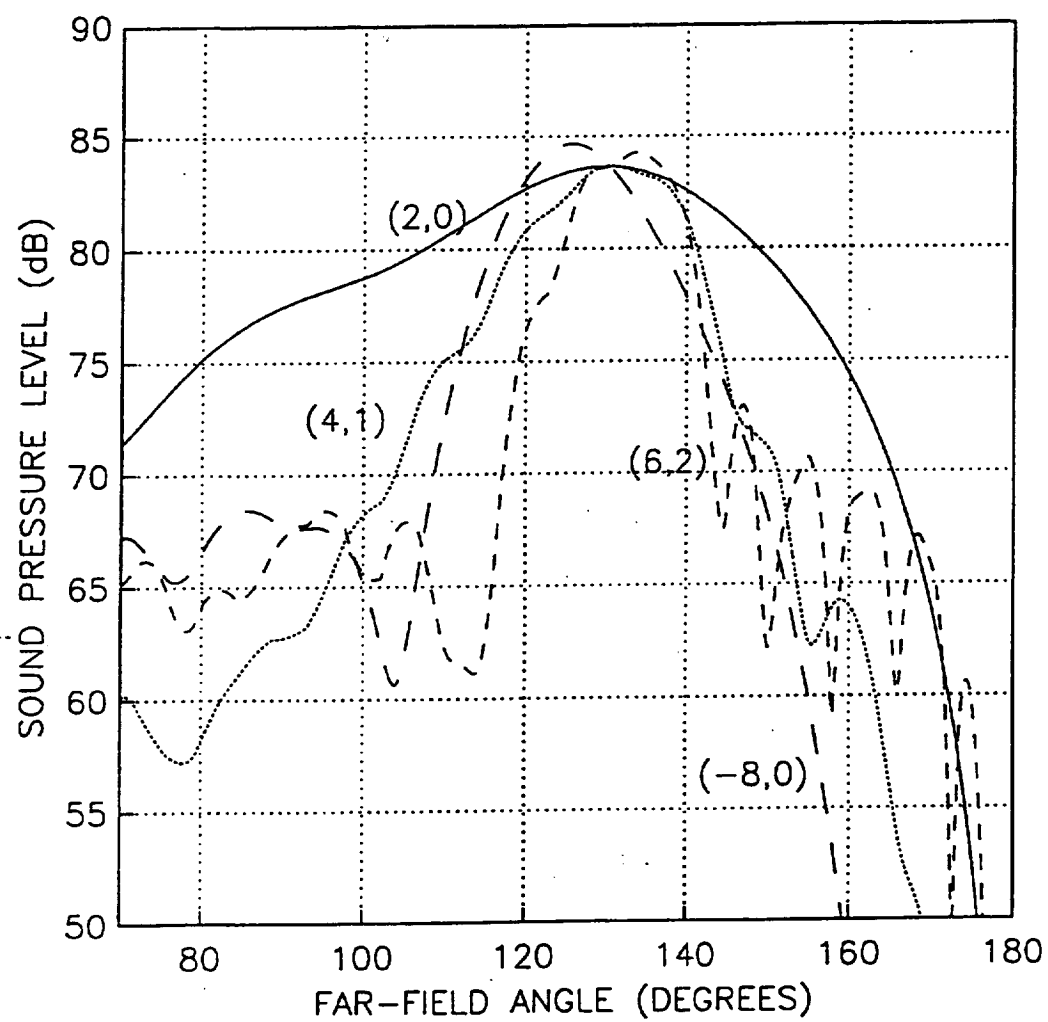
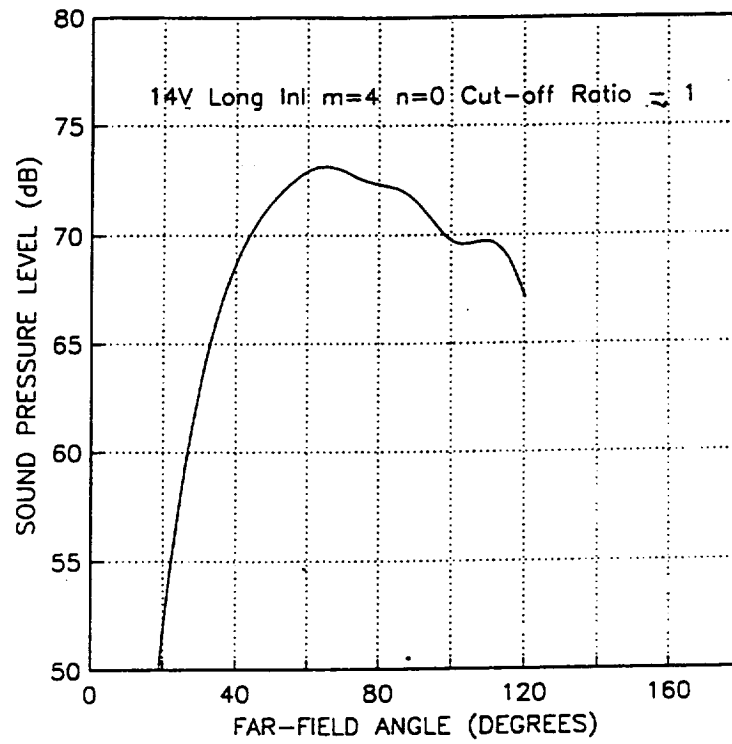
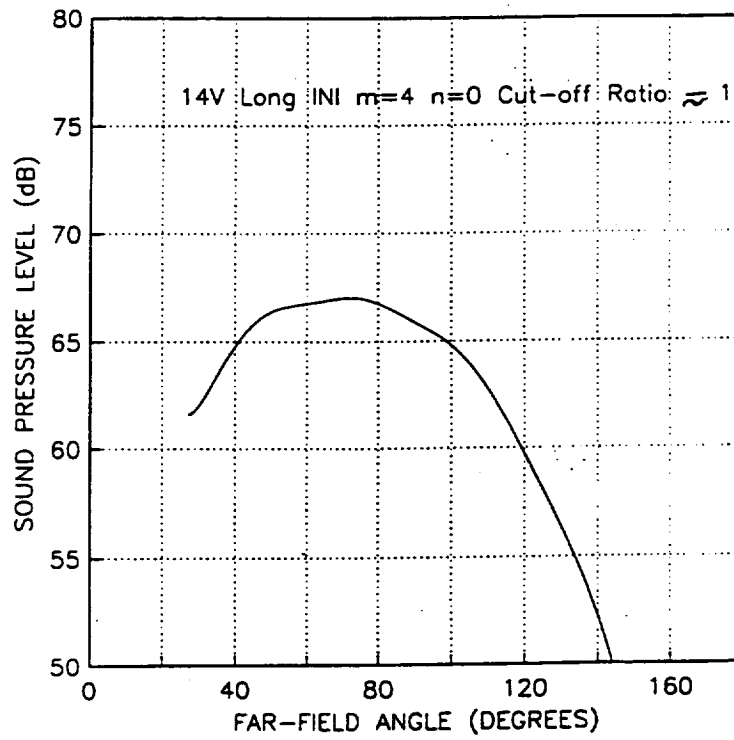


Fig. 18 Far-field shapes at a cut-off ratio of 1.5: Aft

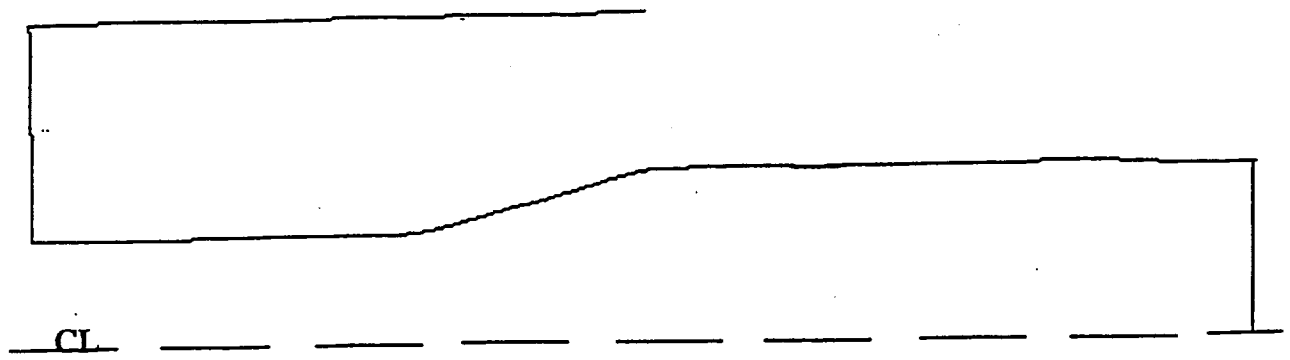


(a)

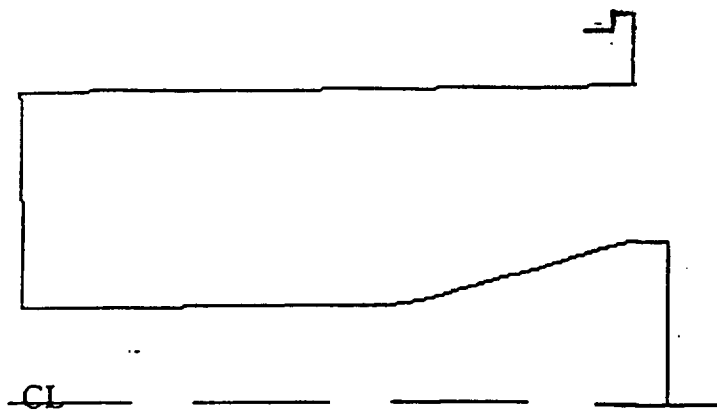


(b)

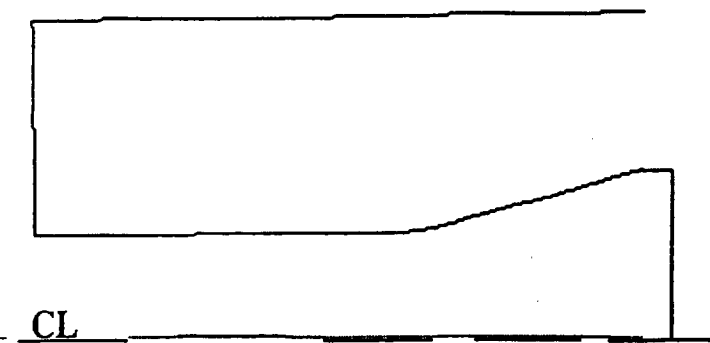
Fig. 19 Far-field shapes at a cut-off ratio of ~ 1 : (a) Inlet (b) Aft



(a) No flange

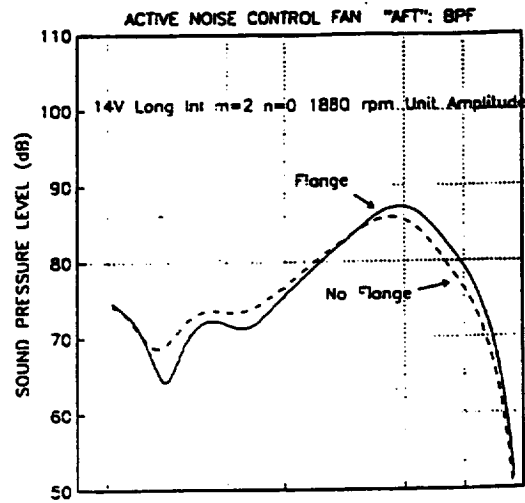


(b) Short center body

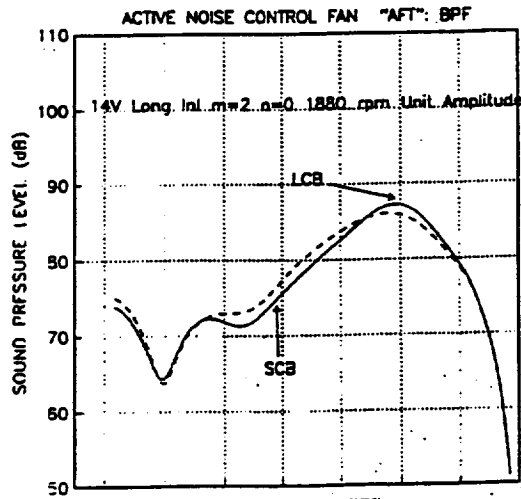


(c) Short center body and no flange

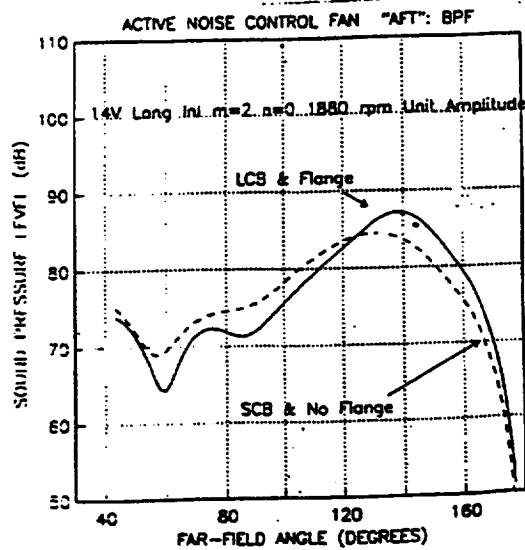
Fig. 20 Aft duct exit geometry variations



(a)

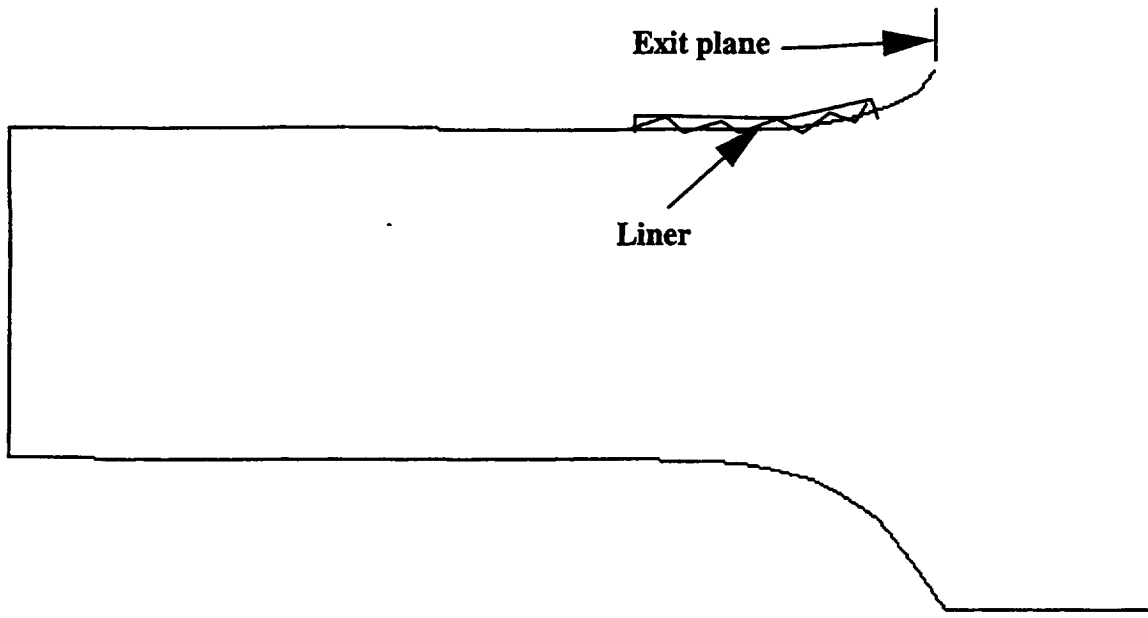


(b)

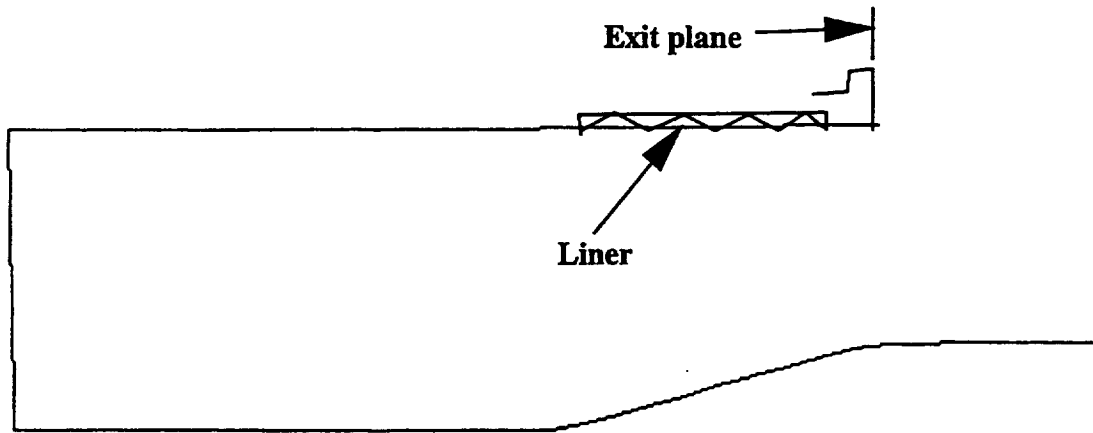


(c)

Fig. 21 Far-field directivity: Effect of aft duct exit geometry
 (a) No flange, (b) Short center body, (c) Short center body and no flange



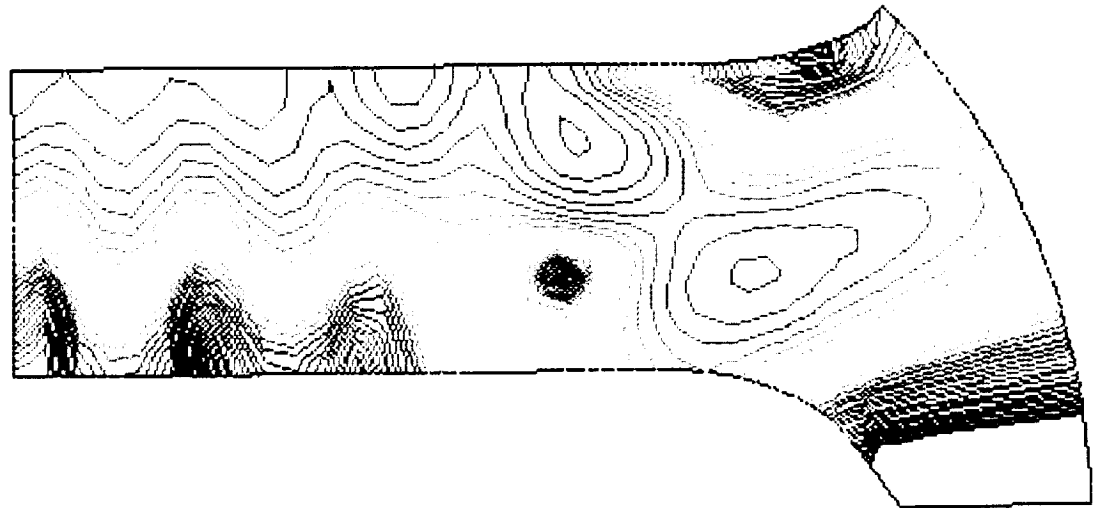
(a) Inlet Duct



(b) Aft Duct

Fig. 22 Liner locations

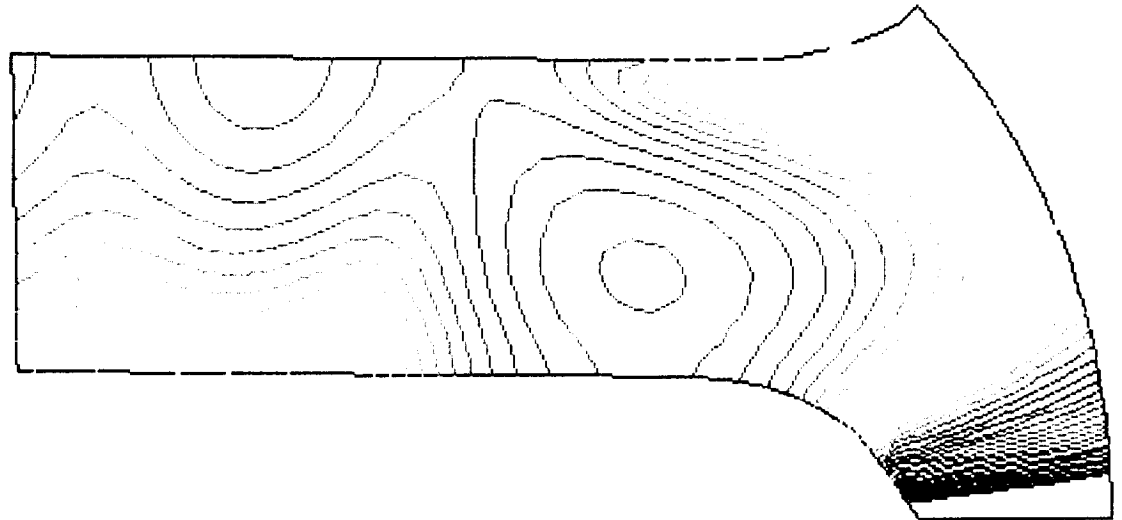
m=2 n=0 BPF



CONTOUR LEVEL:

80.000000
81.000000
82.000000
83.000000
84.000000
85.000000
86.000000
87.000000
88.000000
89.000000
90.000000
91.000000
92.000000
93.000000
94.000000
95.000000
96.000000
97.000000
98.000000
99.000000
100.000000
101.000000
102.000000
103.000000
104.000000
105.000000
106.000000
107.000000
108.000000
109.000000
110.000000
111.000000
112.000000
113.000000
114.000000
115.000000
116.000000
117.000000
118.000000
119.000000
120.000000

m=4 n=0 2BPF

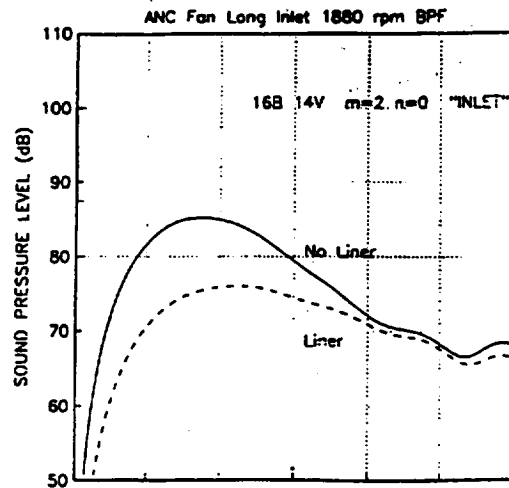


m=6 n=0 3BPF

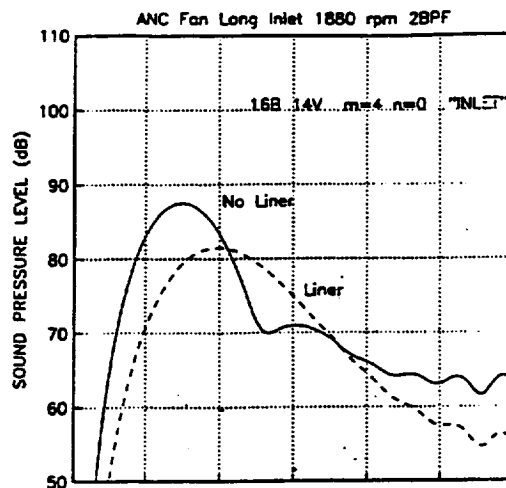


ORIGINAL PAGE IS
OF POOR QUALITY

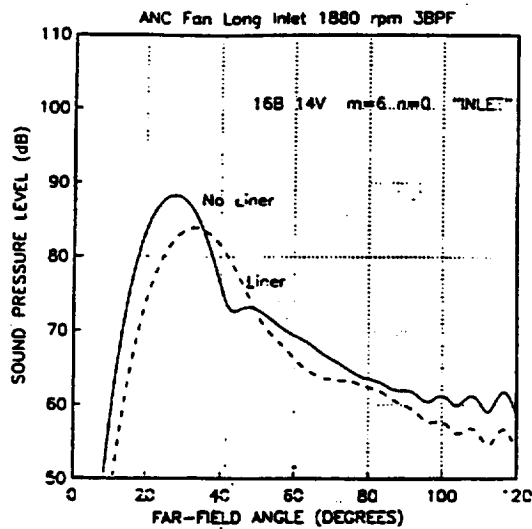
Fig. 23 ANC Fan inlet duct pressure (dB) contours 1886 rpm 16B 14 V
Effect of lining: Impedance $z = 0.45 - i 0.40$



(a)



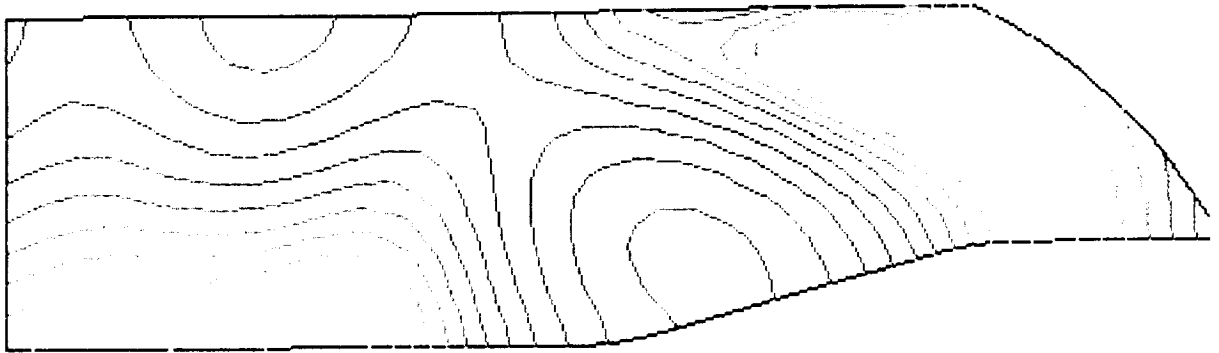
(b)



(c)

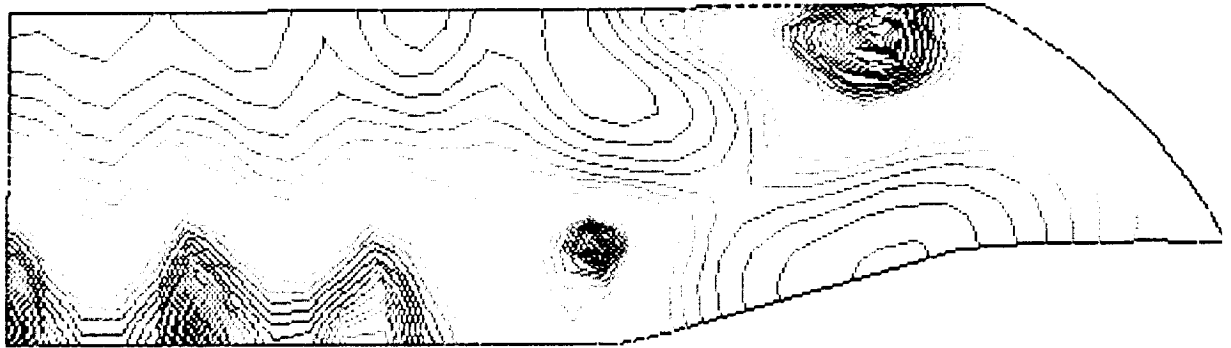
Fig. 24 Far-field directivity: Effect of liner — Inlet
(a) BPF, (b) 2BPF, (c) 3BPF

m=2 n=0 BPF

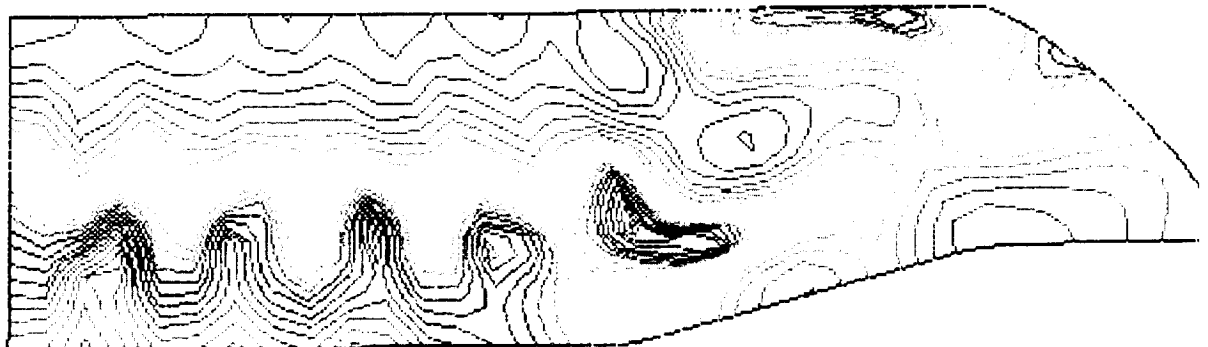


CONTOUR LEVELS

m=4 n=0 2BPF



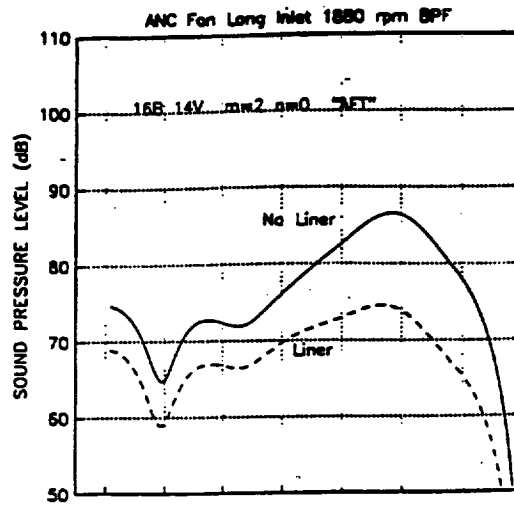
m=6 n=0 3BPF



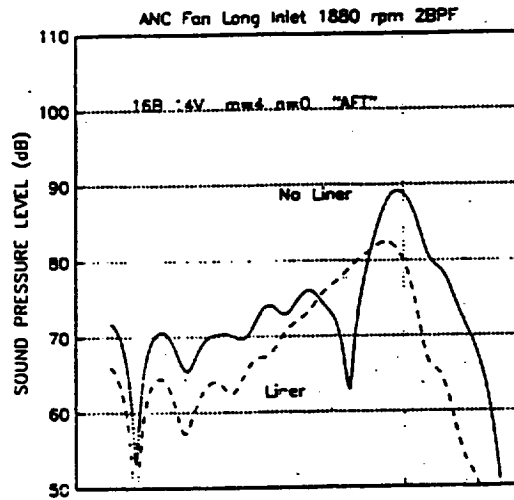
ORIGINAL PAGE IS
OF POOR QUALITY

Fig. 25 ANC Fan aft duct pressure (dB) contours 1886 rpm 16 B 14 V
Effect of lining : Impedance $z = 0.45 - i 0.40$

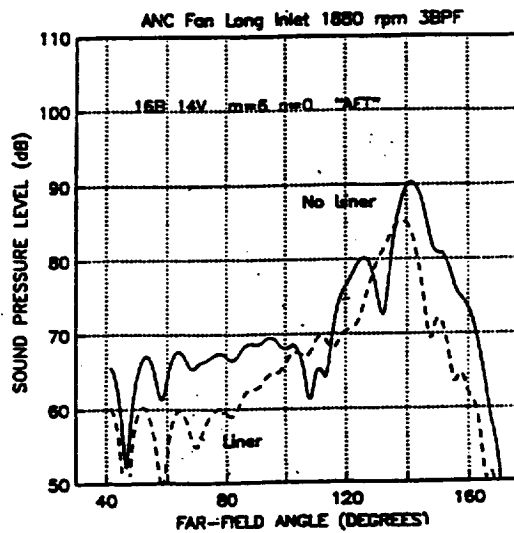
REPORT DOCUMENTATION PAGE			Form Approved OMB No. 0704-0188	
Public reporting burden for this collection of information is estimated to average 1 hour per response, including the time for reviewing instructions, searching existing data sources, gathering and maintaining the data needed, and completing and reviewing the collection of information. Send comments regarding this burden estimate or any other aspect of this collection of information, including suggestions for reducing this burden, to Washington Headquarters Services, Directorate for Information Operations and Reports, 1215 Jefferson Davis Highway, Suite 1204, Arlington, VA 22202-4302, and to the Office of Management and Budget, Paperwork Reduction Project (0704-0188), Washington, DC 20503.				
1. AGENCY USE ONLY (Leave blank)	2. REPORT DATE July 1995	3. REPORT TYPE AND DATES COVERED Final Contractor Report		
4. TITLE AND SUBTITLE Computation of Noise Radiation From Turbofans: A Parametric Study		5. FUNDING NUMBERS WU-538-03-11 C-NAS3-27186		
6. AUTHOR(S) M. Nallasamy				
7. PERFORMING ORGANIZATION NAME(S) AND ADDRESS(ES) NYMA, Inc. 2001 Aerospace Parkway Brook Park, Ohio 44142		8. PERFORMING ORGANIZATION REPORT NUMBER E-9747		
9. SPONSORING/MONITORING AGENCY NAME(S) AND ADDRESS(ES) National Aeronautics and Space Administration Lewis Research Center Cleveland, Ohio 44135-3191		10. SPONSORING/MONITORING AGENCY REPORT NUMBER NASA CR-198359		
11. SUPPLEMENTARY NOTES Project Manager, John F. Groeneweg, Propulsion Systems Division, NASA Lewis Research Center, organization code 2700, (216) 433-3945.				
12a. DISTRIBUTION/AVAILABILITY STATEMENT Unclassified - Unlimited Subject Category 71 This publication is available from the NASA Center for Aerospace Information, (301) 621-0390.			12b. DISTRIBUTION CODE	
13. ABSTRACT (Maximum 200 words) This report presents the results of a parametric study of the turbofan far-field noise radiation using a finite element technique. Several turbofan noise radiation characteristics of both the inlet and the aft ducts have been examined through the finite element solutions. The predicted far-field principal lobe angle variations with duct Mach number and cut-off ratio compare very well with the available analytical results. The solutions also show that the far-field lobe angle is only a function of cut-off ratio, and nearly independent of the mode number. These results indicate that the finite element codes are well suited for the prediction of noise radiation characteristics of a turbofan. The effects of variations in the aft duct geometry are examined. The ability of the codes to handle ducts with acoustic treatments is also demonstrated.				
14. SUBJECT TERMS Acoustics; Far-field radiation; Principal lobe angles; Finite element technique			15. NUMBER OF PAGES 47	
			16. PRICE CODE A03	
17. SECURITY CLASSIFICATION OF REPORT Unclassified	18. SECURITY CLASSIFICATION OF THIS PAGE Unclassified	19. SECURITY CLASSIFICATION OF ABSTRACT Unclassified	20. LIMITATION OF ABSTRACT	



(a)



(b)



(c)

Fig. 26 Far-field directivity: Effect of liner — Aft
(a) BPF. (b) 2BPF. (c) 3BPF